

## ABSTRACT

Title of Document: A PROBABILISTIC-MECHANISTIC APPROACH TO  
MODELING STRESS CORROSION CRACKING  
PROPAGATION IN ALLOY 600 COMPONENTS WITH  
APPLICATIONS

Gary Wu, M.S., 2011

Directed by: Professor Mohammad Modarres, Mechanical Engineering  
Department

Stress corrosion cracking (SCC) is a major degradation mechanism of Alloy 600 steam generator (SG) tubes composed of three main stages: crack incubation, crack initiation and crack propagation. Since SG tubes act as a barrier between the radioactive material and the atmosphere, SCC becomes a critical failure mechanism that jeopardizes safety and integrity. As such, this research proposes a probabilistic-mechanistic approach focused on modeling SCC propagation of Alloy 600 SG tubes with uncertainty. The approach is presented in two parts; the first is an empirical model and the second is a simulation process. To provide a background, this research provides an overview of SCC fundamentals, nuclear power generation and SGs, as well as specifics regarding SG tube degradation. Simulation of SCC on Alloy 600 SG tubes in primary water provided logical results. Future work in this research is also discussed at the end of this paper.

A PROBABILISTIC-MECHANISTIC APPROACH TO MODELING STRESS  
CORROSION CRACKING PROPAGATION IN ALLOY 600 COMPONENTS WITH  
APPLICATIONS

By

Gary Wu

Thesis submitted to the Faculty of the Graduate School of the  
University of Maryland, College Park in partial fulfillment  
of the requirements for the degree of  
Master of Science

2011

Advisory Committee:

Professor Mohammad Modarres, Chair

Professor Jeffrey W. Herrmann

Professor Ali Mosleh

© Copyright by  
Gary Wu  
2011

## **Acknowledgements**

First and foremost, I would like to thank my advisor, Professor Mohammad Modarres, for his continuous assistance, patience, and guidance throughout this thesis development process. Also, I would like to acknowledge my family and friends who were there during the late nights and early mornings to support me in this endeavor. Last, but not least, I would like to thank Mr. Kenneth Karwoski for assisting me in my search for relevant data.

## Table of Contents

Acknowledgements.....	ii
Table of Contents.....	iii
List of Figures.....	v
List of Tables.....	vii
Chapter 1 Introduction.....	1
Chapter 2 Understanding Stress Corrosion Cracking.....	5
2.1 Stress Corrosion Cracking Factors.....	6
2.1.1 Susceptible Material and Corrosive Environment.....	7
2.1.2 Constant Tensile Stress.....	9
2.2 Stages of Stress Corrosion Cracking.....	11
2.3 Stress Corrosion Cracking Mechanisms and Models.....	14
2.3.1 Crack Initiation Mechanisms.....	14
2.3.2 Crack Initiation Models.....	15
2.3.3 Crack Propagation Mechanisms.....	17
2.3.4 Crack Propagation Models.....	20
Chapter 3 Stress Corrosion Cracking of Steam Generator Tubes.....	25
3.1 Nuclear Power Generation.....	25
3.1.1 Pressurized Water Reactor (PWR).....	26
3.1.2 PWR Steam Generators.....	27
3.2 Steam Generator Tube Degradation.....	33
3.2.1 Recirculating Steam Generator Tube Degradation.....	34
3.2.2 Once-Through Steam Generator Tube Degradation.....	37
3.3 US Experience with Steam Generator Tube Ruptures.....	39
3.4 Further Analysis on PWSCC in Steam Generator Tubes.....	41
3.4.1 PWSCC Locations and Orientations.....	41
3.4.2 Overview of Applied and Residual Stresses.....	45
3.4.3 Other PWSCC Conditions in Alloy 600 Tubes.....	45
Chapter 4 Development of Empirical SCC Propagation Model.....	47
4.1 Base Empirical Model.....	48
4.2 Added Factors – pH and Yield Strength.....	50

4.3	Final Proposed Model .....	53
4.4	Model Parameter Estimation Using Experimental Data .....	56
4.4.1	Bayesian Regression Analysis .....	56
4.4.2	Estimating Model Parameters using Alloy 600 Data.....	58
4.4.3	Model Parameter Set Results .....	60
Chapter 5	Simulating PWSCC of Alloy 600 Steam Generator Tubes .....	64
5.1	Crack Propagation Simulation Process .....	64
5.2	Initial Assumptions and Distributions.....	67
5.2.1	Steam Generator Assumptions/Conditions .....	68
5.2.2	Initial Crack Length and Depth Distributions.....	70
5.2.3	Model Parameter Set Distributions .....	71
5.3	Failure Criteria .....	72
5.4	Simulation Results and Findings.....	73
Chapter 6	Conclusion .....	82
Chapter 7	Future Work.....	86
Appendix A	– Experimental Data.....	87
Appendix B	– WinBUGS Code .....	89
Appendix C	– MATLAB Code.....	91
Bibliography	.....	98

## List of Figures

Figure 2.1 - (a) Intergranular crack: Caustic SCC in the HAZ of Type 316L Stainless Steel NaOH reactor vessel (b) Transgranular Crack: SCC in 308 Stainless Steel Weld in Aqueous Chloride at 95C [8] .....	6
Figure 2.2 - Required combination of factors for stress corrosion cracking [7].....	7
Figure 2.3 - Crack propagation curve (log of crack growth rate versus stress intensity factor) [9] .....	11
Figure 2.4 - Schematic representation of the stages of SCC; crack length versus duration [10].....	12
Figure 2.5 - Schematic diagram of the film-rupture mechanism with dissolution driven crack advancement [9] .....	18
Figure 2.6 - Schematic diagram of film-rupture mechanism with mechanically driven crack advancement [9] .....	18
Figure 2.7 - Surface mobility theory cracking mechanism [16] .....	19
Figure 2.8 - Graph portraying current characteristics of slip-dissolution at crack tip [18] .....	21
Figure 2.9 - Surface mobility theory cracking mechanism. Adapted from [16].....	22
Figure 3.1 - Schematic of PWR power plant [24] .....	26
Figure 3.2 - Cutaway view of a Westinghouse recirculating steam generator [25].....	29
Figure 3.3 - Cutaway view of a Babcock & Wilcox once-through steam generator [25]	30
Figure 3.4 - Schematic diagram of recommended B and Li concentrations in primary water [28].....	33
Figure 3.5 - Schematic of RSG tube degradation mechanisms [30].....	34
Figure 3.6 - Schematic of tube degradation mechanisms in OTSGs [24] .....	38
Figure 3.7 - Overview of PWSCC cracking locations and orientations [24].....	42
Figure 3.8 - PWSCC initiated by denting at tube support plate interactions [24] .....	44
Figure 3.9 - Tube pinching due to denting at the tube support plate causing PWSCC at the U-Bend apex [24].....	44
Figure 4.1 - CPR versus 1/T graph [36].....	49
Figure 4.2 – Crack propagation rate as a function of pH at different K values .....	50
Figure 4.3 - Yield Strength as a function of Cold Work Percentage .....	52

Figure 4.4 – Crack propagation rate as a function of yield strength.....	53
Figure 4.5 - Crack propagation data for Alloy 600 in primary water .....	58
Figure 4.6 – Marginal distributions for Stage I model parameters and s.d.....	61
Figure 4.7 - Marginal distributions for Stage II model parameters and s.d. ....	61
Figure 4.8 – Calculated crack propagation rate for PWSCC of Alloy 600 in (pH - 7.3, $\sigma_{ys}$ = 389MPa) .....	63
Figure 5.1 - Crack propagation simulation flow chart.....	65
Figure 5.2 - Initial crack length distribution for simulation [44].....	70
Figure 5.3 - Semi-elliptical crack penetrating through tube wall [19].....	71
Figure 5.4 - Crack Propagation Rate as a function of Stress Intensity Factor for simulation.....	75
Figure 5.5 – Crack propagation rate versus stress intensity factor for 300°C, 315°C .....	76
Figure 5.6 - Crack depth as a function of time .....	77
Figure 5.7 – "Time-to-100%TWE" Distribution .....	77
Figure 5.8 - Overlapping Time-to-100% Through-Wall Extent Distributions.....	78
Figure 5.9 - Aggregated Time-to-100% Through-Wall Extent Distribution.....	79
Figure 5.10 - Time Required for Leak Rate to Exceed Specified Limit for Multiple Cracks .....	81



## List of Tables

Table 2.1- Common Material-Environment Combinations Susceptible to SCC [6] .....	8
Table 3.1 - Summary of steam generator operating conditions .....	28
Table 3.2 - Typical compositions of Alloy 600 and Alloy 690 [27].....	31
Table 3.3 - Estimated operating and residual stress levels at affected locations .....	45
Table 4.1 - Yield strengths for Alloy 600 at various cold work percentages [36].....	51
Table 4.2 - Breakdown of incorporated SCC factors in final model .....	54
Table 4.3 - Material and Environmental Conditions for experimental data used.....	59
Table 4.4 - Uniform Priors for Stage I model parameters .....	59
Table 4.5 - Uniform Priors for Stage II model parameters .....	60
Table 4.6 - Summary of Stage I and Stage II model parameter distributions.....	62
Table 5.1 - Steam Generator Mechanical/Environmental Properties .....	68
Table 5.2 - PWSCC Region Assumptions .....	69
Table 5.3 – Initial assumptions used in simulation.....	71
Table 5.4 - PWSCC location probability .....	74

## Chapter 1 Introduction

From a physical perspective, degradation is inherent in all objects that exist on this planet. This ranges from living objects, including plants and animals to inanimate objects such as raw materials, which are used to create everyday items. In general, researchers and theorists have taken long strides in defining and classifying degradation mechanisms. The understanding of degradation mechanisms in turn provides information on how to eliminate or retard degradation. For metals, a set of core mechanical degradation mechanisms have been defined and accepted including deformation, fracture, impact, creep, thermal shock, wear, buckling, corrosion, and fatigue. [1] Other degradation mechanisms can be formulated by combining the core mechanisms such as corrosion fatigue and stress corrosion cracking. It is important to mention that, while corrosion does not mechanically degrade, it often leads to mechanical failure.

Among all of the degradation mechanisms, stress corrosion cracking (SCC) is notable as it is known to cause catastrophic failure with little to no warning due to the combination of corrosion and cracking under specific stresses. [2] Primarily, the materials that are susceptible to SCC are metal alloys in their respective corrosive environments. For instance, SCC has been diagnosed as the mechanism for component degradation in the nuclear industry, where nickel-based alloys such as Alloy 600 are used extensively. In particular, SCC is a major contributor to Alloy 600 steam generator tube cracking in nuclear power plants. Since the steam generator tubes essentially act as a barrier between the radioactive material and the environment, catastrophic and

unexpected failure of these tubes could result in unplanned power plant shutdowns. More importantly, it could allow for a radioactive release to the atmosphere.

With the worldwide shift towards zero-emission energy production, nuclear energy has become a promising alternative to coal and oil. Thus, the safety and integrity of nuclear power plants and its components have never been more important. Over the past four decades, SCC has been degrading steam generator tubes in operation and in turn reducing the reliability of nuclear power plants. In the nuclear industry, the short term effects of SCC on steam generator tubes include reduced power generation efficiency, unplanned downtime, increased maintenance costs, radioactive outbreaks and more. Long term effects of SCC on the steam generator tubes include a permanent power generation efficiency decrease and a tarnished reputation in the event of a radioactive release. Evidently, the long-term consequences of SCC are much less forgiving than the short term effects since a single radioactive outbreak could shift public perspective on the safety of nuclear power. For instance, the consequences of nuclear power plant mishaps in the events of Three Mile Island (1979) and Chernobyl (1986) are still felt today by the nuclear industry.

As such, understanding the SCC mechanism is critical to reducing the probability of unexpected and detrimental failures in susceptible mechanical systems, specifically in the nuclear industry. Stress corrosion cracking involves multiple stages including crack incubation, crack initiation, and crack propagation. Crack incubation can be defined as the period when the crack forms from a defect-free surface. Crack initiation is the longest period where the crack grows very slowly to a threshold size. The propagation stage is the period of degradation immediately before mechanical failure and is often very rapid.

While the crack incubation and crack initiation period takes up most of the degradation process, there is still much debate over their driving mechanisms. As such, it is very difficult to develop or use physics-based models to estimate the crack growth rate. On the other hand, there has been much research on developing deterministic models that predict the crack propagation of steam generator tubes fabricated out of a nickel-based alloy, Alloy 600. [3] Some models [4] are extremely detailed such that they could be used to predict, not only stress corrosion cracking of steam generator tubes, but also stress corrosion cracking of other components as well. Meanwhile, other SCC models are developed empirically using experimental data [5] and only applicable to steam generator tubes. However, all of the models ultimately only provide a single value prediction of SCC growth rate given the components' operating conditions. Thus, in order to comprehend the entire SCC degradation mechanism, it is logical to start with understanding and modeling the crack propagation stage with uncertainty measures.

This research aims to develop an approach to model stress corrosion crack propagation of Alloy 600 with uncertainty measures by adapting to existing mechanistic models and simulating degradation growth. A probabilistic-mechanistic approach developed here provides a framework by which the life of Alloy 600 components can be estimated in the form of a distribution. Unlike in single value estimation, distributions provide not only the mean values, but also the shape and magnitude of the uncertainty around the mean values. In this research, the developed approach is applied to Alloy 600 steam generator tubes in primary water conditions.

In addition to the probabilistic-mechanistic approach to modeling crack propagation, this research also aims to provide a background on stress corrosion cracking,

nuclear power generation, steam generators, steam generator tube degradation, as well as SCC in steam generator tubes specifically.

This thesis first explores the complex fundamentals of stress corrosion cracking in Chapter 2 by describing the factors that induce SCC, the multiple stages of SCC, and the mechanisms and models. Chapter 3 provides a background on nuclear industry and explores SCC of steam generator tubes. Chapter 4 describes the developed empirical model used in the probabilistic-mechanistic approach to predicting SCC propagation of Alloy 600 and Chapter 5 applies this model to SCC of Alloy 600 steam generator tubes in primary water. Finally, Chapter 6 provides a discussion on the approach as a whole and Chapter 7 offers recommendations for future work.

## Chapter 2 Understanding Stress Corrosion Cracking

While it is accepted that stress corrosion cracking (SCC) is highly complex, the definition of this phenomenon is inherent in its name. In general, SCC can be defined as a delayed cracking mechanism which occurs only with susceptible materials in a corrosive environment under a constant tensile stress. Any deviation from these three required aspects will not result in a case of stress corrosion cracking. The first occurrence of stress corrosion cracking was observed in the nineteenth century with the failure of brass cartridge cases for firearms in ammonia-bearing environments. It was found later that ammonia resulting from the organic matter decomposition with high humidity was a key contributor to SCC. [6] Another early case in the 1920s was the cracking of carbon steel boilers in steam-engine locomotives resulting in explosions. During that time period, these two cases of material failure were defined as “season cracking” and “caustic embrittlement,” respectively. [7] Since then, the SCC phenomenon and the susceptible combinations of material, stress and environment have been studied extensively. The mechanism is of particular interest because it often occurs under normal service conditions and can result in catastrophic failure, often with little or no warning. [2] Depending on the specific combination of factors, stress corrosion cracks can initiate and propagate intergranularly (along the grain boundaries) or transgranularly (through the grain boundaries). Figure 2.1a and Figure 2.1b show the examples of intergranular and transgranular cracks, respectively. [8] Figure 2.1a shows an SCC crack in the heat-affected zone (HAZ) of Type 316 stainless steel in NaOH reactor vessel. Figure 2.1b shows a SCC crack in a 308 stainless steel weld in aqueous chloride. Generally, SCC is observed in material-environment-stress combinations that result in film formation on the

material surface. This film may be passivating layers, tarnish films, or dealloying layers. While these layers reduce a material's susceptibility to uniform corrosion, they in turn increase its SCC susceptibility. [9]

This Chapter further explores the factors affecting SCC, stages of SCC, possible SCC mechanisms, and proposed SCC crack propagation models.



**Figure 2.1 - (a) Intergranular crack: Caustic SCC in the HAZ of Type 316L Stainless Steel NaOH reactor vessel (b) Transgranular Crack: SCC in 308 Stainless Steel Weld in Aqueous Chloride at 95C [8]**

## 2.1 Stress Corrosion Cracking Factors

As the definition of SCC implies, the three critical factors in SCC are: a susceptible material, a specific corrosive environment, and a constant surface tensile stress. This required combination of conditions is often portrayed and understood through Figure 2.2.

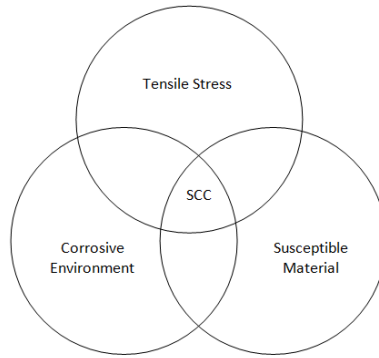


**Figure 2.2 - Required combination of factors for stress corrosion cracking [7]**

### **2.1.1 Susceptible Material and Corrosive Environment**

In order for SCC to occur, there must be a material with a certain microstructure that is susceptible to a particular corrosive environment. Since these two factors complement each other, it is logical to explore them as a cohesive factor.

Even though SCC has been exhibited in various types of materials, SCC usually refers to the degradation of metals. It has been accepted that, while not immune, pure metals are much less susceptible to SCC than alloys with the same base metal. [6][7] In most cases, this is irrelevant since pure metals are not used frequently due to their low strength as compared to alloys. Alloys that are known to be susceptible to SCC include the following: carbon steels, stainless steels, nickel alloys, copper alloys, aluminum alloys, titanium alloys, zirconium alloys and magnesium alloys. Each of the susceptible alloy materials can be matched up to specific corrosive environments. These SCC-inducing environments are normally in aqueous form and a part of the bulk solution. Table 2.1 provides examples of some material/environment combinations.



**Table 2.1- Common Material-Environment Combinations Susceptible to SCC [6]**

<b>Alloys</b>	<b>Environments</b>
Stainless Steels	Chlorides; caustic; polythionic acids; water + O <sub>2</sub>
Nickel Alloys	Hot caustic; molten chlorides; polythionic acids; high-temperature water and steam contaminated with O <sub>2</sub> , Pb, Cl <sup>-</sup> , F <sup>-</sup> , or H <sub>2</sub> S
Cooper Alloys	Ammonia; fumes from HNO <sub>3</sub> ; SO <sub>2</sub> in air + water vapor; mercury
Aluminum Alloys	Aqueous solutions especially with halogen ions; water; water vapor; N <sub>2</sub> O <sub>4</sub> ; HNO <sub>3</sub> ; oils; alcohols; CCl <sub>4</sub> ; mercury
Titanium Alloys	Red fuming HNO <sub>3</sub> ; dilute HCl or H <sub>2</sub> SO <sub>4</sub> ; methanol and ethanol; chlorinated or brominated hydrocarbons; molten salt; Cl <sub>2</sub> ; H <sub>2</sub> ; HCl gas

It can be seen in the common material-environment combinations that an environment that causes SCC in one alloy does not necessarily cause SCC in different alloy. This aspect is agreeable with basic corrosion fundamentals.

The matching corrosive environments are not limited to a single configuration. Many parameters influence the final environmental composition, which alters the susceptibility of the material-environment combination. Some of these parameters include: temperature, solute species, solute concentration, pH, electrochemical potential, and solution viscosity.[2][9] Changing any one of these parameters could either increase or decrease the SCC susceptibility due to the corrosion requirements. For instance, if the electrochemical potential is shifted away from the corrosion range, the material-environment combination becomes much less susceptible to SCC. On the other hand, if the temperature is increased, the SCC susceptibility usually becomes much higher. [6] It is important to note here that the exact composition of the bulk solution environment can differ significantly from that at the crack tips. As such, altering the environmental

parameters of the bulk solution does not necessary translate to the same change in parameters at the crack tip.[9]

In the same way that environments are affected by numerous parameters, materials can also be defined by a set of metallurgical parameters that affect its SCC susceptibility. Some of these metallurgical parameters include: grain boundary microstructure and segregation, cold work (strain-hardening), thermal treatment (distribution of carbides), residual stress, and grain size. [3] Depending on the material and its complementary corrosive environment, altering the condition of any one of these parameters could increase or decrease the SCC susceptibility. In the case of austenitic stainless steels, sensitization may cause the formation of chromium carbides at the grain boundaries and subsequently the depletion of chromium from the surrounding areas. As a result, the material is susceptible to intergranular SCC. On the other hand, non-sensitized austenitic stainless steels have been known to fail due to transgranular cracking. [2] However, since chromium carbides provide extra strength, the sensitized austenitic stainless steels are less susceptible to SCC than non-sensitized austenitic stainless steels.

Evidently, environmental and material conditions as defined by each respective set of parameters greatly affect the material-environment susceptibility to SCC. By changing conditions slightly such as heat-treating the material to achieve a carbide precipitation and reducing the temperature of the environment, the probability of SCC occurring can be reduced.

### **2.1.2 Constant Tensile Stress**

Aside from a susceptible material and a corrosive environment, the third factor required for SCC is a constant tensile stress. The total stress that contributes to SCC is the

arithmetic sum of externally applied stress and the residual stresses in the metal.

Externally applied stresses are usually the stresses from normal operating conditions such as the reaction stress from pressure differentials in a pressure vessel. Applied stresses alone are generally not driving factors in SCC susceptibility as they are minimal in comparison to macroscopic yield stress. On the other hand, localized residual stresses from manufacturing and conditioning acts usually increase the total stress to a value closer to or above the material yield stress.[6]

Unlike corrosion fatigue which is caused by the combination of cyclic stress and a corrosive environment, stress corrosion cracking requires a static tensile or torsional load to open and sustain a crack. The minimum stress required for SCC propagation is often described by a threshold stress intensity factor ( $K_{ISCC}$ ), a value that is different for every SCC scenario. [9]The stress intensity factor is a function of the total stress and the crack length. In short, failure due to SCC does not occur until the stress intensity factor reaches  $K_{ISCC}$  for the particular material-environment-stress combination. Figure 2.3 shows a typical crack propagation curve with a threshold stress intensity factor. While cracking occurs at stress intensity factors less than  $K_{ISCC}$ , the crack growth rate at this stage is sustained at a low magnitude (less than  $10^{-13}$  meters per second in some cases) and thus becomes negligible. The stages of SCC are further explained in Section 2.2.

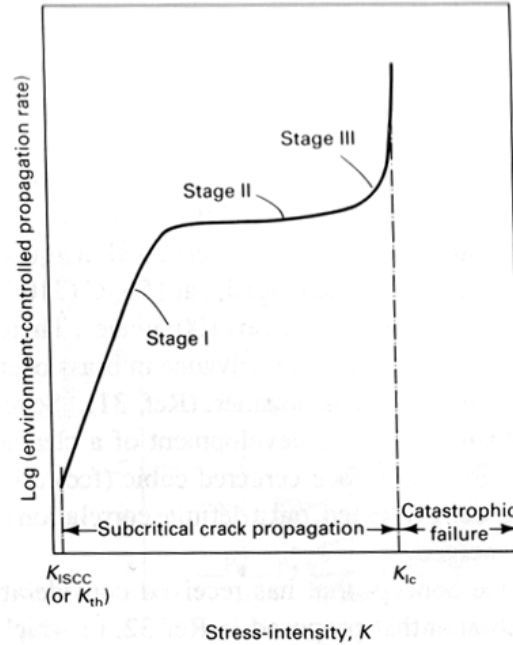


Figure 2.3 - Crack propagation curve (log of crack growth rate versus stress intensity factor) [9]

## 2.2 Stages of Stress Corrosion Cracking

Among the stages of SCC, the most studied in research is often the crack propagation to failure stages. This is because the crack propagation stages are usually very abrupt and contribute almost entirely to the rapid catastrophic failures. Nevertheless, it is important to understand the mechanistic progression to SCC starting from a smooth surface of a material to its 100% through-wall failure. Figure 2.4 is a schematic representation of the stages of SCC as shown in a crack length versus time graph.

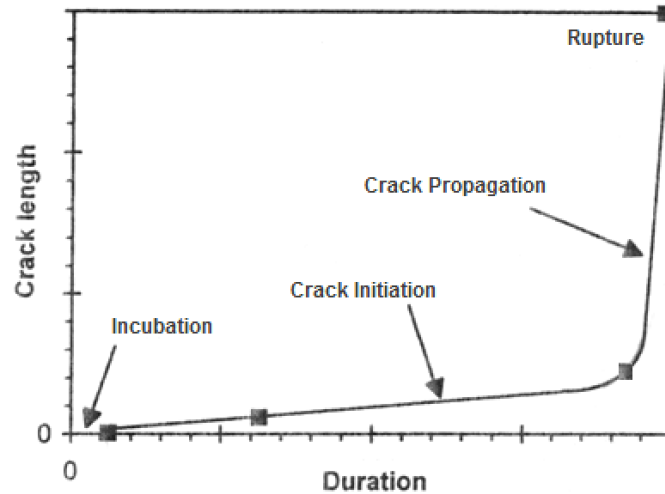


Figure 2.4 - Schematic representation of the stages of SCC; crack length versus duration [10]

From the mechanical perspective, SCC can be segmented into four stages: incubation, crack initiation, crack propagation and rupture. The schematic representation in Figure 2.4 demonstrates that most of the SCC time resides in the incubation and crack initiation stages. Crack propagation is shown to be extremely fast as compared to the prior two stages. Since the rupture stage is immediate, it can be described as the end of crack propagation in this explanation.

The incubation period of SCC is defined as the establishment of corrosion cracking conditions. These include parameters from all three of the SCC factors such as electrochemical potential, temperature, pH, concentration, microstructure conditions and stress. As such, the incubation time period is not a set value but varies depending on the material-environment-stress combination. For instance, if the total stress applied (external applied + residual stress) is below the yield stress of the material, the incubation period can be much longer. [10] Brisson et al. [11] estimated an incubation period (time to crack initiation) of ~540 hours for intergranular SCC in Alloy 600 (nickel-based alloy).

The crack initiation period of SCC takes up the longest duration as shown in Figure 2.4. Also known as the “slow-propagation” period, the duration of crack initiation

can range from a few hundred hours to approximately twenty years or more. [10] The crack length increases during this period at a very slow rate as driven once again by the material-environment-stress parameters focusing on mechanical loading, temperature, material strength (carbide precipitation and surface condition). As mentioned earlier, the crack growth rate at the crack initiation stage is very slow. If a crack does not reach the threshold stress intensity in the component's lifetime, SCC is considered negligible for that particular crack. However, at a critical threshold value of stress intensity,  $K_{ISCC}$ , the crack initiation stage transitions to the rapid crack propagation stage where the crack growth rate increases significantly. In the case of SCC in Alloy 600 steam generator tubes, Scott et al. [5] has determined a  $K_{ISCC}$  threshold value of 9 MPa $\sqrt{m}$  using data published by McIlree et al. [12].

During the crack propagation stage, the stress corrosion cracks become macroscopic and propagate very quickly as compared to the crack initiation stage. This stage can be further segmented into three separate stages as shown previously in Figure 2.3. After the threshold stress intensity factor has been reached, the crack propagation enters Stage I where the stress intensity values are relatively low. In Stage 1 propagation, the crack growth rate increases rapidly with the increase of stress intensity. At a particular stress intensity factor, Stage I begins to transition to Stage II, where the crack growth rate ideally becomes constant and independent of stress intensity. The transition stress intensity level varies once again depending on the material-environment-stress combination. [9] While crack growth rate in Stage 2 is schematically represented to be virtually independent of the increase in stress intensity, quantitative data [9] show that there is a weak stress dependence in practice. Stage III of the crack propagation period

can be seen as negligible since the crack growth rate spikes very quickly, causing material rupture at  $K_{IC}$ .

Generally, the incubation stage can be grouped with crack initiation stage and the rupture stage can be grouped with the crack propagation stage.

## **2.3 Stress Corrosion Cracking Mechanisms and Models**

As described in Section 2.1, the SCC mechanism can ultimately be understood as two separate but sequential stages: crack initiation and crack propagation. A couple mechanisms have been proposed for crack initiation while a plethora of mechanisms have been proposed for crack propagation. Both crack initiation and propagation model are also explored in this section.

### **2.3.1 Crack Initiation Mechanisms**

While this process is less studied than crack propagation, it has been proposed that stress corrosion cracks can initiate from macroscopically smooth surfaces at surface discontinuities, corrosion pits and by intergranular corrosion or slip dissolution. [9]

Surface discontinuities in materials can be the result of manufacturing and fabrication flaws. These flaws may include but are not limited to: grooves, laps, and burrs. Moreover, these same flaws can be induced by way of wear during regular service. Stress corrosion cracks can also initiate from pits as the material is subjective to a corrosive environment. When the electrochemical potential exceeds the pitting potential, pitting occurs on the metal as the protective film is broken down. It is important to note that, while pits can form on the material in a corrosive environment, pits do not always transition to a stress corrosion crack. Certain parameters must be existent including a large enough pit aspect ratio (pit depth to pit length) and the right electrochemistry such

that a passivation layer forms. [9] Aside from initiation from pits or surface flaws, stress corrosion cracks can initiate on a smooth surface by intergranular corrosion or slip-dissolution when grain boundary chemistry differs significantly from the bulk solution.[9]

Evidently, the exact mechanism for SCC initiation is still unknown. In practice, certain material-environment scenarios could be susceptible to a combination of all the mechanisms. Moreover, it is difficult to determine in-situ or experimentally when pits become cracks or when intergranular corrosion becomes intergranular stress corrosion cracking.

### 2.3.2 Crack Initiation Models

Despite the fact that the exact mechanism for SCC initiation is still unclear, a few models have been developed for SCC initiation. For the most part, the models are specific to a single mechanism or designed for specific material-environment combinations. Two models are described here as examples.

Turnbull et al. [13] developed a model based on deterministic equations for simulating the evolution of pit depth at different exposure times and for the percentages of pits that transition to stress corrosion cracks. The evolution of pits is described by the following equation:

$$\frac{\partial P(x, t)}{\partial t} = -\frac{\partial}{\partial x} [g(x)P(x, t)] + S(P(x, t), x, t)$$

where  $P(x, t)$  is the pit size distribution function,  $g(x)$  is the pit growth rate, and  $S(P(x, t), x, t)$  is the number of pits of size in range  $x \rightarrow x+\delta x$  nucleated or deactivated in a given area during time interval  $\delta t$ .



The pit depth is defined by:

$$x = \alpha t^\beta$$

where  $\alpha$  and  $\beta$  are parameters as determined by experimental data. Thus, by deriving the equation for pit depth, the pit growth rate is defined by:

$$\frac{dx}{dt} = g(x) = \beta \alpha^{1/\beta} x^{(1-\frac{1}{\beta})}$$

Adopting the pit-to-crack transition criteria of Kondo [14] such that the transition occurs when the crack growth rate by mechanical driving force is greater than the pit growth rate. The crack growth rate is given by:

$$\frac{dx}{dt} = C \sigma^p x^q$$

where  $\sigma$  is the applied stress,  $x$  is the flaw depth, and  $\{C, p, q\}$  are experimentally determined parameters. The researchers subsequently applied this model to a specific case of steel steam turbine discs exposed to a number of environments. As described, this model assumes that stress corrosion cracks initiate first as pits in steam turbine disc steels.

Aly et al. [15] proposed a new approach to assess crack initiation of primary water stress corrosion cracking occurring in Alloy 600 control rod drive mechanism (CRDM) nozzles. The model is the superposition of electrochemical and fracture mechanics models. The model developed is described by:

$$t_i = 4.88 \times 10^{-23} \cdot \exp\left(\frac{32822.35}{T}\right) \cdot \ln\left(1.79 \left(\frac{278.5}{\sigma}\right)\right)$$

where  $t_i$  is the time to initiation in days,  $T$  is the temperature in Kelvin, and  $\sigma$  is the applied stress in MPa. This semi-empirical model was then validated using experimental data and literature data.

An acceptable generic model for SCC initiation has yet to be developed due to the various different initiation mechanisms proposed. However, initiation models for specific scenarios can provide researchers and stakeholders with the ability to predict the SCC timeline from smooth surface to mechanical fracture with more certainty.

### 2.3.3 Crack Propagation Mechanisms

Even though there is a plethora of proposed mechanisms, a couple mechanisms emphasized in literature will be explored in this section.

Many dissolution mechanisms have been proposed to explain the SCC propagation. However, most of these mechanisms have converged to the film-rupture (also known as slip-dissolution) mechanism. [9] In a corrosive environment, a protective passivation layer forms on the metal surface. The film-rupture mechanism proposes that crack propagation rate is related to the amount and rate of metal dissolution that occurs on the bare metal surface when the passivation layer is ruptured by the applied stress. When stress localizes at the crack tip and the protective layer is ruptured, there is an anodic dissolution reaction at the exposed bare metal. The bare metal repassivates and the protective film is once again ruptured. This process repeats until mechanical fracture. There are also slight variations to this mechanism such as the tarnish-rupture, which assumes that the crack advancement is driven mechanically by rupture, rather than driven chemically by dissolution. In both cases, the repeated passivation-rupture-repassivation process occurs. Figure 2.5 shows a schematic diagram of the film-rupture process as

driven by anodic dissolution. Figure 2.6 shows a schematic diagram of the same process as driven by mechanical rupture.

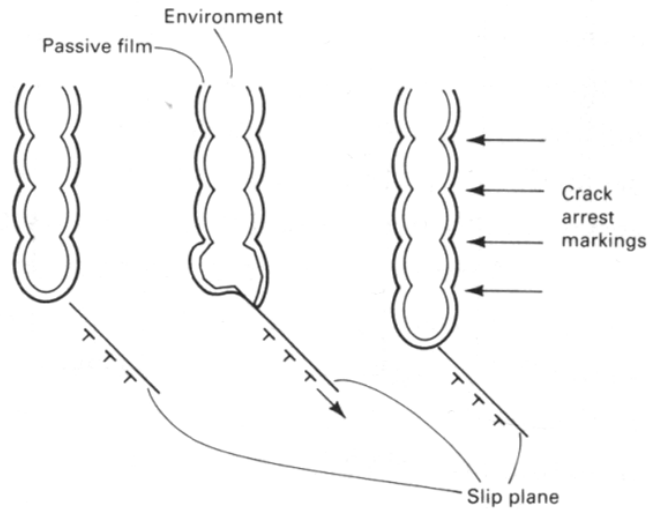


**Figure 2.5 - Schematic diagram of the film-rupture mechanism with dissolution driven crack advancement [9]**

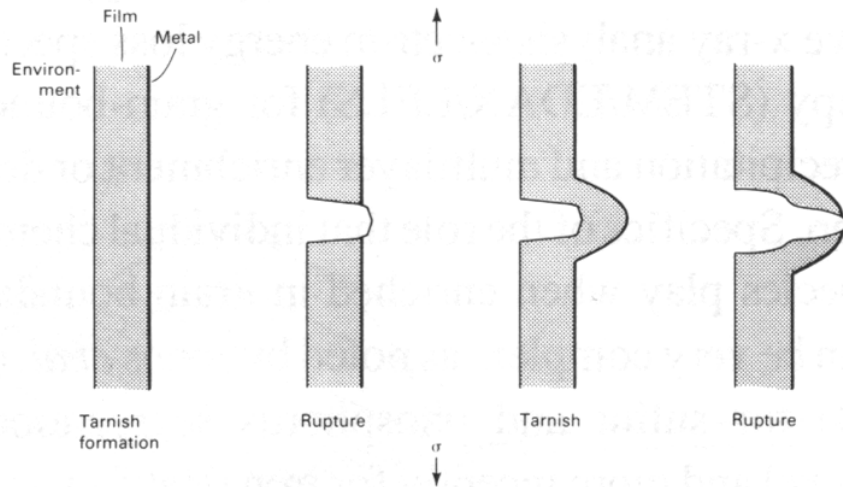


**Figure 2.6 - Schematic diagram of film-rupture mechanism with mechanically driven crack advancement [9]**

Another mechanism is the surface mobility theory, where it has been postulated [16] that SCC propagation is related to the change in surface self-diffusivity of the metal by the corrosive environment. The mechanism assumes a metal under tensile stress will relax the stresses by growing cracks if the surface mobility is high enough. The

researchers also postulated that the material-environment combinations susceptible to SCC cause an increase in surface mobility. If the surface mobility is high enough, the cracks will grow to relieve stresses one atom at a time. Figure 2.7 shows a schematic representation of the surface mobility theory.

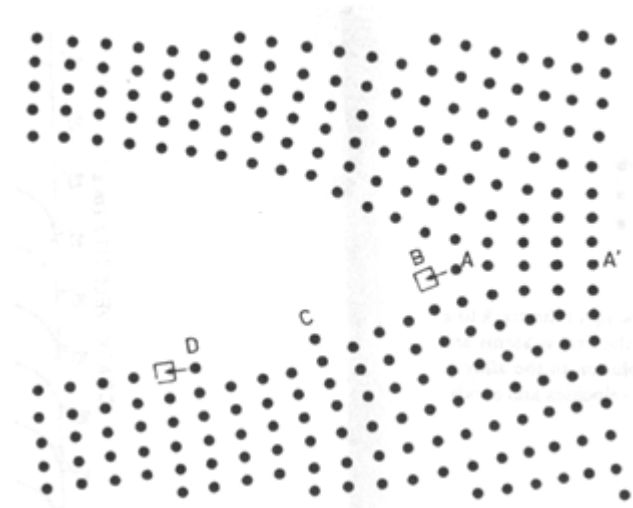


**Figure 2.7 - Surface mobility theory cracking mechanism [16]**

As stresses concentrate at the crack tip, it will favor the A-B atomic shift which advances the crack one atomic distance. The crack progresses through B-C-D at a specific rate, which is the rate-determining step of this mechanism. Finally, as the atom progresses from B to D, it will provide a location for new A-B exchanges. The crack propagates along the A-A' plane in the schematic. In practice, this place could be located through or along grain-boundaries causing trans- or inter-granular SCC, respectively.

Other SCC propagation mechanisms include, but are not limited to, internal oxidation and hydrogen embrittlement. Internal oxidation is proposed SCC propagation mechanism [3] developed for Alloy 600 in primary water conditions based on embrittlement due to a layer of oxygen atoms on the grain boundaries, or to the formation of high pressure gas bubbles ( $\text{CO}/\text{CO}_2$ ). In some materials such as ferritic steels, nickel-base alloys, aluminum alloys, and intermetallic compounds, hydrogen embrittlement has

been suggested as the SCC propagation mechanism. [9] This mechanism proposes that grain-boundary segregation is accelerated as hydrogen dissolves into the alloy.

### 2.3.4 Crack Propagation Models

Researchers have developed a variety of crack propagation models to quantitatively determine the crack growth rate in the propagation stage. Some models are generic and are designed for all material-environment-stress combinations, while others are developed for specific SCC scenarios. Additionally, some models are inherently mechanistic as they are derived from postulated crack mechanisms (as described in Section 2.3.3) while others have been developed empirically. This section addresses both types of models.

A well-known model that describes SCC for a generic set of material-environment-stress combinations is derived from the film-rupture/slip-dissolution crack mechanism. The first model of this type was developed by F.P Ford and P.L Andresen[17], but was later enhanced to include effects of material tensile properties and changing in strain rate caused by a moving crack to crack growth rate. This enhanced model was proposed by T. Shoji et al.[4] and named the Fracture Research Institute (FRI) model. Attributing the crack growth rate to the rate of metal dissolution at the crack tip, the model describes SCC crack propagation using the following equation:

$$\dot{a} = \frac{M}{z\rho F} \cdot \frac{i_o(t_o)^m}{(1-m)(\varepsilon_f)^m} \cdot (\dot{\varepsilon}_{ct})^m$$

where:  $\dot{a}$  – crack growth rate

$\rho$  – mass density

$i_o$  – current density of a bare surface

$m$  – slope of current density curve

$M$  – atomic weight

$z$  – number of electrons oxidized

$t_o$  – time at start of repassivation

$\varepsilon_f$  – fracture strain of oxide film

$\dot{\epsilon}_{ct}$  – crack-tip strain rate

In this equation, the SCC crack growth rate is governed primarily by 'm', the slope of the current density curve and ' $\epsilon_f$ ', crack-tip strain rate. The slope of the current density curve is directly related to the film repassivation rate which can be described by the following equation and visually portrayed in Figure 2.8.

$$i = i_o \cdot \left(\frac{t}{t_o}\right)^{-m}$$

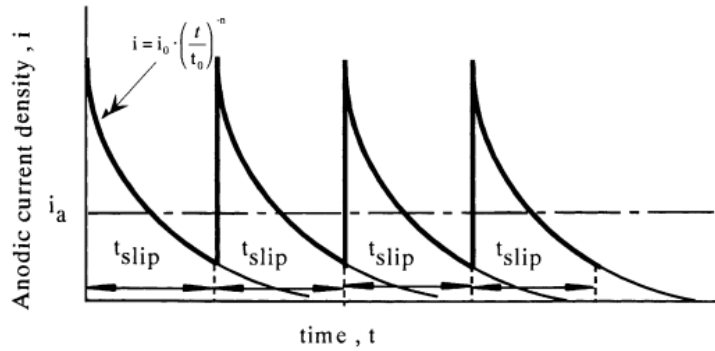


Figure 2.8 - Graph portraying current characteristics of slip-dissolution at crack tip [18]

Since experiments have shown that the crack-tip strain rate is not a measurable parameter [17], T. Shoji et al. [4] derived the following mechanically-based strain rate equation:

$$\dot{\epsilon}_{ct} = \frac{\beta \sigma_y n}{E(n-1)} \cdot \left(2 \frac{\dot{K}_I}{K_I} + \frac{\dot{a}}{r_o}\right) \left\{ \ln \left[ \frac{\lambda}{r_o} \left(\frac{K_I}{\sigma_y}\right)^2 \right] \right\}^{1/(n-1)}$$

where: $E$ – young's modulus	$n$ – strain hardening coefficient
$\sigma_y$ – yield stress	$\beta$ – dimensionless constant
$K_I$ – stress intensity factor (SIF)	$\dot{K}_I$ - rate of change of SIF
$r_o$ – distance ahead of crack tip	$\lambda$ – dimensionless constant

By substituting the strain rate equation into the crack growth rate equation, it can be seen that the FRI model for predicting SCC propagation is rather extensive.

A quantitative model was also developed with the proposition of the surface mobility theory cracking mechanism. Jose Galvele [16] assumed an energy value is required to create a vacancy in a stressed region is equivalent to:

$$U = \sigma a^3$$

where  $U$  is the energy required to create a vacancy in a stressed region,  $\sigma$  is the stress applied to an atom, and  $a$  is the length of an atom. By thermodynamic equilibrium,

Galvele proposed that the crack growth rate can be described by the following equation:

$$V_p = \frac{D_s}{L} \left[ \exp\left(\frac{\sigma a^3}{kT}\right) - 1 \right]$$

where:  $V_p$  – crack growth rate  
 $L$  – vacancies diffusion distance  
 $D_s$  – surface self-diffusion coefficient  
 $k$  – Boltzmann constant  
 $T$  – temperature

The variable  $L$  is defined as the diffusion distance of the adatoms or vacancies as shown in Figure 2.9. In some cases,  $L'$  is used if the atoms are diffused into the environment before arriving to the kink site at D.

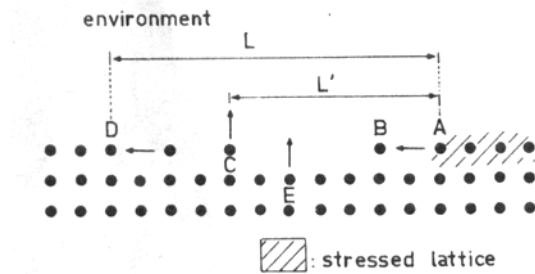


**Figure 2.9 - Surface mobility theory cracking mechanism. Adapted from [16].**

Among all of the driving variables in the model, the surface self-diffusion coefficient ( $D_s$ ) is the most volatile since the applied stress, the size of atoms and temperature values can be approximated with much more certainty. Researchers [16] have developed an equation

for all stress corrosion crack scenarios to estimate the surface self-diffusion coefficient based on the ratio between operating temperature and material melting temperature as given by:

$$D_s = 7.4 \times 10^{-2} \exp\left(-\frac{30 T_m}{RT}\right) + 1.4 \times 10^{-6} \exp\left(-\frac{13 T_m}{RT}\right)$$

where  $R$  is the gas constant and  $T_m$  is the melting point of the material.

Scott [5] developed an empirical model for predicting stress corrosion crack growth of Alloy 600 in primary water using data published by Smailowska et al. [12]. This empirical model is based off the idea that SCC propagation can be represented by a power-law, similar to the Paris equation for fatigue. Using data for a typical primary water chemistry of 2ppm Li, 1200ppm B (yielding a pH of 7.3), Scott proposed the following equation:

$$\frac{da}{dt} = 2.8 \times 10^{-11} (K - 9)^{1.16}$$

where  $\frac{da}{dt}$  is the crack growth rate and  $K$  is the stress intensity factor assuming  $9\text{MPa}\sqrt{\text{m}}$  as the threshold stress intensity factor ( $K_{\text{ISCC}}$ ). Since its development, the equation and its estimated parameters have been referenced extensively for SCC of Alloy 600 in primary water. [3][19][20] Some developed computer programs have even implemented this model for estimating crack propagation for Alloy 600 materials. [21]

The Electric Power Research Institute (EPRI) also developed an empirical model for Alloy 600.[20] The developers recommend that the model be used to predict the SCC propagation rate in thick-wall components fabricated from Alloy 600 material such as reactor vessel head nozzles. The equation is presented as follows:

$$\dot{a} = \alpha \cdot \exp\left[-\frac{Q}{R}\left(\frac{1}{T} - \frac{1}{T_{ref}}\right)\right] \cdot (K - K_{th})^\beta$$



where:  $\dot{a}$  – crack growth rate                       $Q$  – activation energy for propagation  
 $R$  – universal gas constant                       $T$  – operating temperature  
 $T_{ref}$  – reference temperature                       $K$  – stress intensity factor (SIF)  
 $K_{th}$  – threshold SIF                       $\alpha$  – crack growth amplitude parameter  
 $\beta$  – model parameter

EPRI researchers assumed a value of 1.16 for  $\beta$  and  $9\text{MPa}\sqrt{\text{m}}$  for the threshold stress intensity factor as derived by Scott [5]. It can be seen that this model takes the form of a power-law relationship for the stress dependence and utilizes an Arrhenius model to account for the temperature dependence of SCC.

## **Chapter 3 Stress Corrosion Cracking of Steam Generator Tubes**

As nuclear energy becomes increasingly prevalent worldwide with the shift towards zero-emission power generation, the reliability and integrity of nuclear power plants become more important. Over the last four decades, SCC has been jeopardizing the reliability of nuclear power plants by directly affecting steam generator components. This chapter provides an overview of nuclear power generation, steam generator tube degradation, and the specific phenomenology of PWSCC in steam generator tubes.

### **3.1 Nuclear Power Generation**

Shortly after World War II, the United States began to research peaceful uses of nuclear materials under the Atomic Energy Commission. Since the ground break of the first commercial nuclear power plant in 1958, nuclear power has been a growing source of energy all around the world.[22] As of the year 2009, the United States houses a total of 104 commercial nuclear reactors, collectively generating 8.43 quadrillion BTUs of electricity; approximately 20% of the nation's total electricity. [23] United States commercial nuclear reactors are composed of two different types of reactors: boiling water reactors (BWRs) and pressurized water reactors (PWRs). Of the 104 reactors, 35 of them are BWR and 69 of them are PWRs. The major difference between BWRs and PWRs is that PWRs utilize steam generators to convert heat energy from the nuclear reactor to steam used to generator electricity at the turbine. The steam generator also acts as a barrier between two closed loops, one of which contains radioactive particles. On the other hand, BWRs generate steam directly from the reactor vessel. Since this research is

focused on SCC propagation in steam generator tubes, this section further explores the mechanics of a PWR.

### 3.1.1 Pressurized Water Reactor (PWR)

In a PWR, the power generation can be regarded as two major systems that interact through the steam generator. Figure 3.1 shows a schematic of a typical PWR.

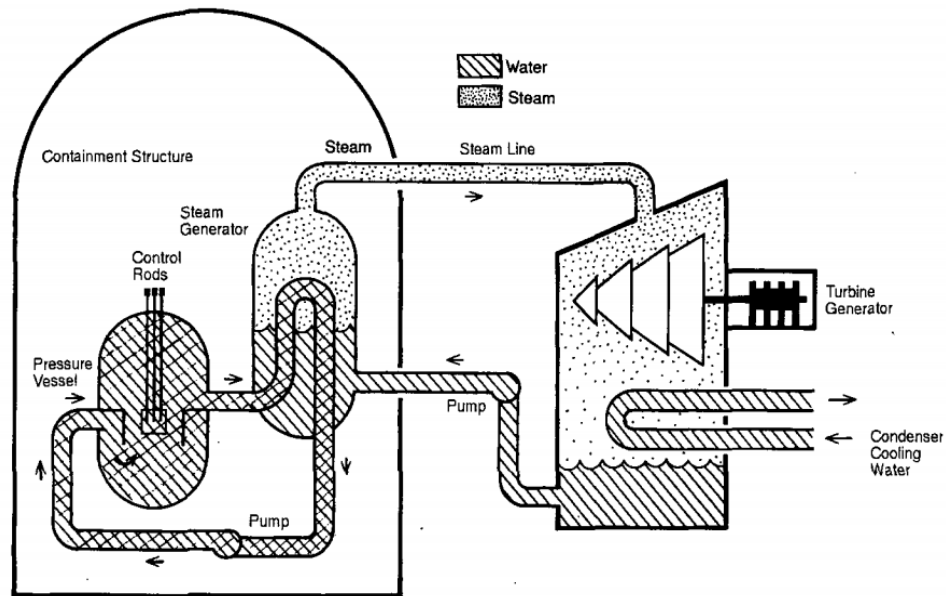


Figure 3.1 - Schematic of PWR power plant [24]

The primary system resides within the containment structure and starts with the reactor vessel. Heat from the fuel is transferred to the coolant (water) and is pumped into the steam generator. At the steam generator, the primary and secondary systems interact and the heat from the water is transferred thus reducing the temperature of the coolant leaving the steam generator. At the steam generator, the heat from the coolant boils water and produces steam. This steam is part of the secondary system and leaves the steam generator towards the turbine generator where it is converted into electricity. After passing through the turbine, the steam is condensed into water and is pumped back into the steam generator for reuse. Depending on the required power output of the nuclear

reactors, there may be more than one steam generator used in power generation. For instance, Westinghouse has designed nuclear power plants with up to four steam generators. [25]

### 3.1.2 PWR Steam Generators

Needless to say, steam generators in primary water reactors are extremely crucial to nuclear power plant efficiency. As a heat exchanger, it is ideal for a steam generator to transfer as much heat energy to the secondary side as possible. Meanwhile, steam generators also act as barriers between the reactor core and the outside environment. The integrity of this barrier is critical to preventing radioactive particles from being expelled into the atmosphere. However, degradation in steam generators has been seen in many locations including in steam generator tubes, nozzles as well as in the shell itself.

Hot primary coolant water enters the steam generator from the reactor pressure vessel at a pressure of approximately 15.5MPa and 310°C - 330°C. [24] Once inside the steam generator, the hot coolant flows into thousands of small thin-walled tubes. Concurrently, the secondary feed-water flows around the outside of the tubes picking up heat at a controlled pressure between 5.35MPa and 7.24MPa. [24] The feed-water picks up enough heat from the primary coolant to boil and turn into steam. When the primary coolant leaves the steam generator after the heat exchange, the temperature has been reduced to approximately 288°C. [24] The entrance and exits of primary coolant at the steam generator are often referred as the "hot-leg" and "cold-leg", respectively. Table 3.1 summarizes the pressure and temperature conditions for the primary and secondary side in a typical PWR steam generator.

**Table 3.1 - Summary of steam generator operating conditions**

	<b>Pressure [MPa]</b>	<b>Temperature [°C]</b>
<b>Primary-side (coolant)</b>	15.5	310-330
<b>Secondary-side (feed-water)</b>	5.35-7.24	288

There are two different designs that are used in PWRs today: recirculating steam generators (RSGs) and once-through steam generators (OTSGs). Figure 3.2 shows a cutaway view of a typical Westinghouse recirculating steam generator.

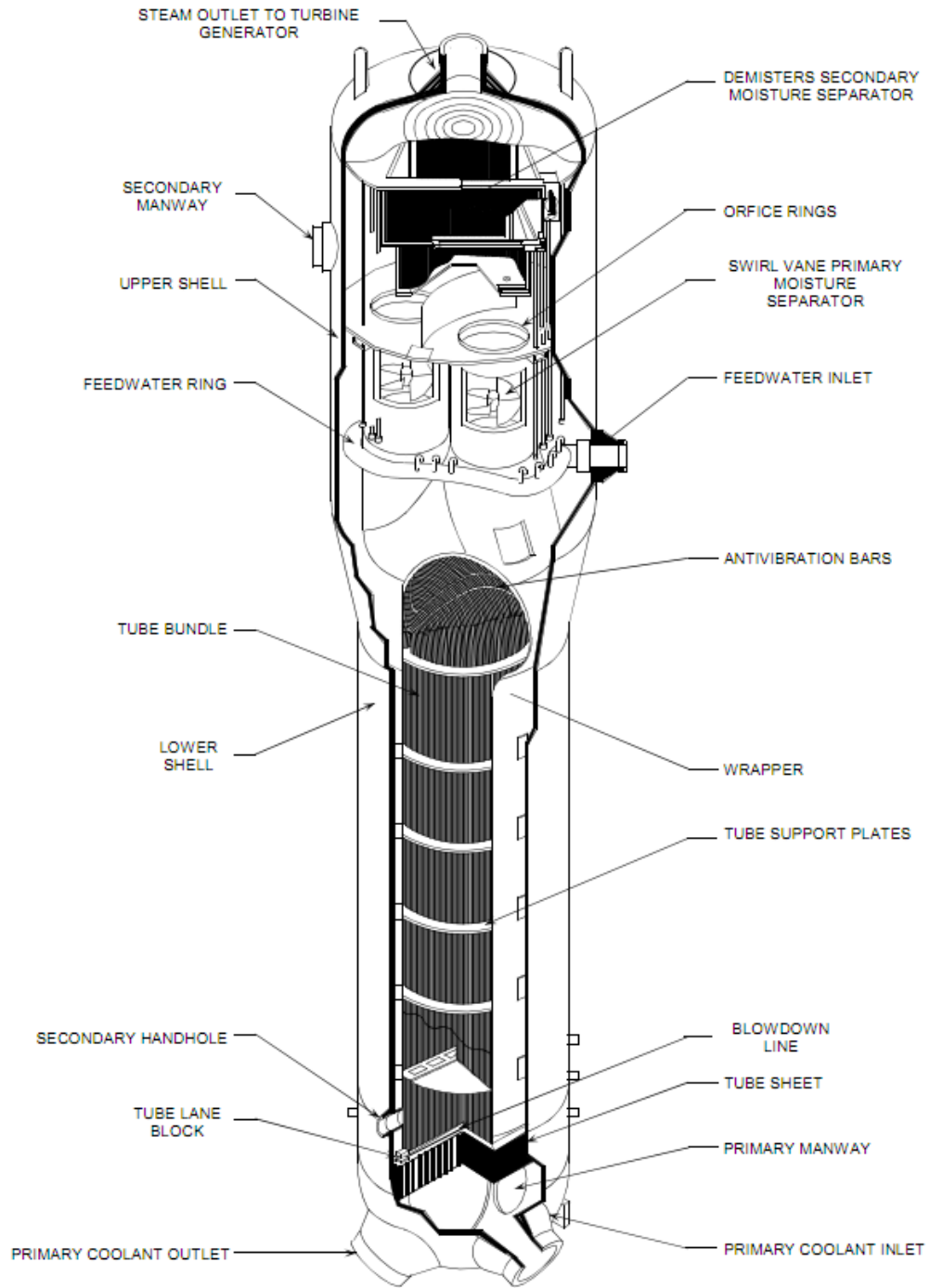


Figure 3.2 - Cutaway view of a Westinghouse recirculating steam generator [25]

As shown in the cutaway, the primary coolant enters the steam generator, gets fed into the U-bend tubes, and exits at the bottom again. The feed-water enters from the side and

the steam exits from the top. Figure 3.3 shows a cutaway view of a Babcock & Wilcox once-through steam generator.

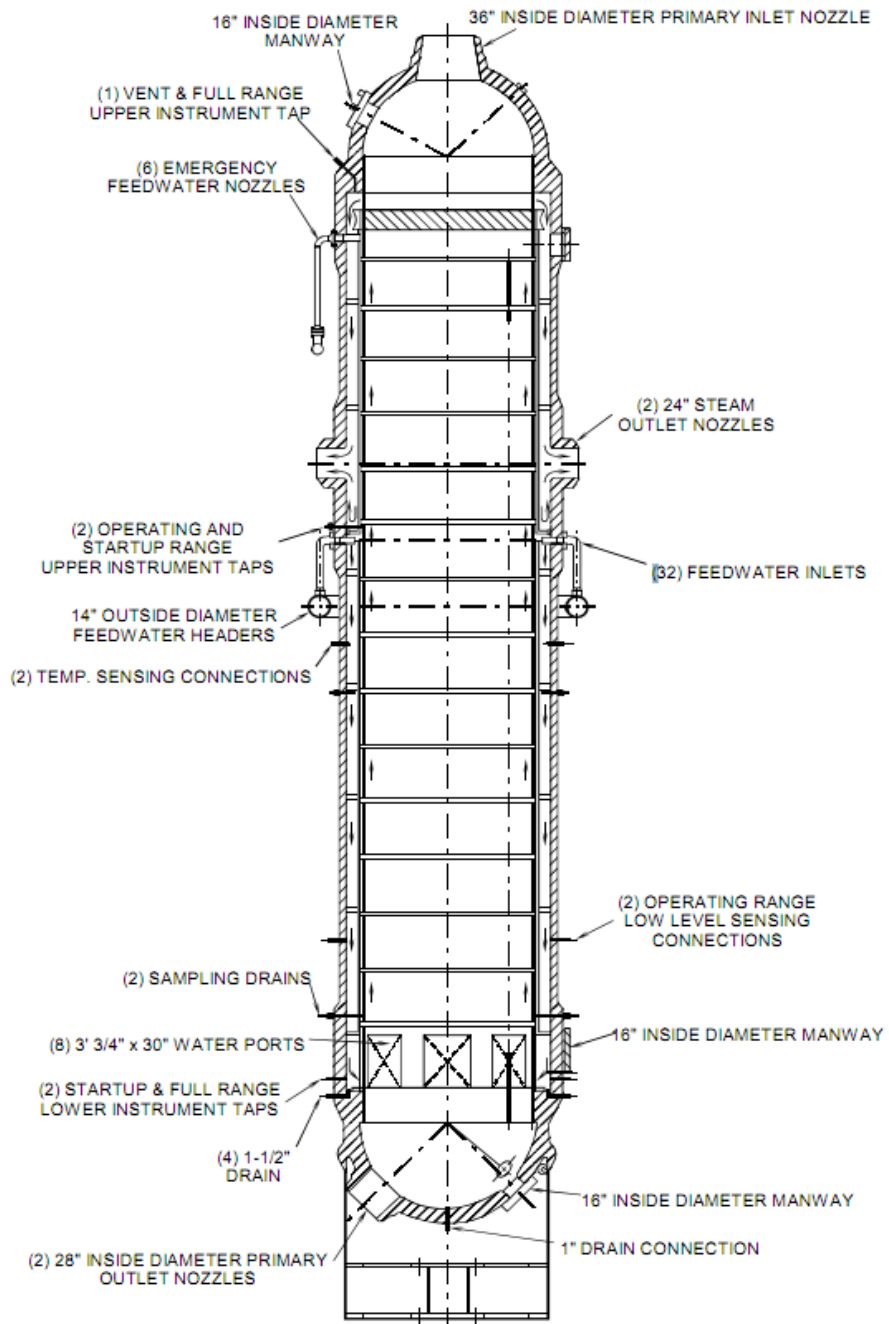


Figure 3.3 - Cutaway view of a Babcock & Wilcox once-through steam generator [25]

As shown in the Figure 3.3, the primary coolant enters at the top and exits at the bottom. Meanwhile, both the feed-water inlet and steam outlets are located on the side of steam generator.

Steam generators, both RSGs and OTSGs, are very large in size and can measure up to 70 feet in height and weigh as much as 800 tons.[23] The number of tubes in a steam generator varies depending on the nuclear power plant, but some steam generators can house up to 30,000+ tubes. For instance, a Babcock & Wilcox steam generator at the Arkansas Nuclear 1 plant has a total of 31,062 tubes. [26] Each tube is about 18 millimeters in diameter and usually no more than 2 mm thick. [25]. The tubes are lined up in a tight bundle and secured laterally by tube support plates. Originally, these tube support plates were fabricated using by drilling holes into solid plates. Eventually, the manufacturers started using a grid like system to avoid denting (See Section 3.2.1.2). Tubes are secured laterally by the tube support plates but not axially. At the tubesheets, however, the tubes are expanded into the plates in order to achieve a seal.

The two types of materials currently used to fabricate steam generator tubes in United States are Alloy 600 and Alloy 690. These tubes are generally heat treated, either by mill-annealing (MA) or thermally-treating (TT), in order to achieve more desirable mechanical and corrosion-resistant properties. Typical compositions of Alloy 600 and Alloy 690 are shown in Table 3.2.

**Table 3.2 - Typical compositions of Alloy 600 and Alloy 690 [27]**

% wt.	Ni	Cr	Fe	C	S	Mn	Si	Cu
<b>Alloy 600</b>	72.0 min	14.0- 17.0	6.00- 10.00	0.15 max	0.015 max	1.00 max	0.50 max	0.50 max
<b>Alloy 690</b>	58.0 min	27.0- 31.0	7.0- 11.0	0.05 max	0.01 max	0.5 max	0.50 max	0.50 max



Of the 69 steam generators, 10 of them use Alloy 600MA tubing, 17 of them use Alloy 600TT, and 42 of them use Alloy 690TT. During the 1970s, majority of the nuclear power plants used Alloy 600MA to fabricate steam generator tubes. However, as the tubes began demonstrating degradation, replacement steam generators were equipped with Alloy 600TT tubes to improve corrosion resistance in the 1980s. While Alloy 600TT did not exhibit the same degradation characteristics as Alloy 600MA did a decade prior, plants decided to utilize Alloy 690TT as tube material for replacement steam generators after 1989. Alloy 690 is believed to be even more corrosion resistant than Alloy 600TT due to not only the significant increase in chromium content (twice the amount of Alloy 600), but also the decrease in carbon content.

Water chemistry in steam generators have been improved and altered for the last few decades in order to achieve corrosion resistance and the highest heat transfer. On the primary side, the coolant is primary water with concentrations of boric acid, lithium hydroxide and hydrogen. According to the PWR primary water chemistry guidelines [28], the pH is controlled by both the boron and lithium content. Typically, the boron and lithium concentrations are kept within the shaded band shown in Figure 3.4 in order to keep a pH value of between 6.9 and 7.4.

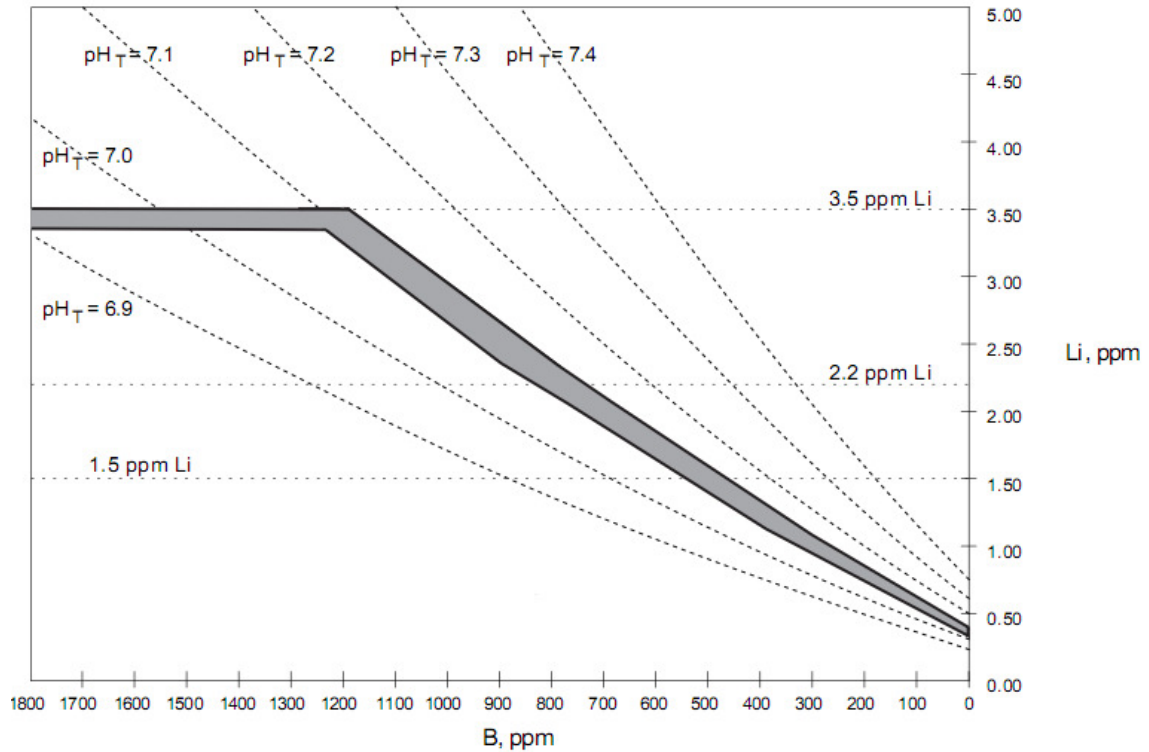


Figure 3.4 - Schematic diagram of recommended B and Li concentrations in primary water [28]

Dissolved hydrogen is maintained at a certain concentration in order to reduce the concentration of dissolved oxygen in the primary water. Dissolved oxygen increases the susceptibility of corrosion formation and also SCC. In order to minimize this concentration, it has been found that amount of dissolved hydrogen is maintained between 25-35cc H<sub>2</sub>/kg H<sub>2</sub>O. [28] On the secondary side, the fluid is all-volatile-treated feed-water maintained at a pH of approximately 9.3. [24]

### 3.2 Steam Generator Tube Degradation

Over the years, steam generator tube degradation in both RSGs and OTSGs has evolved due to the perpetual efforts for preserving steam generator tube integrity shifting from primarily wastage (wall-thinning) and denting up until the 1980 and to a majority stress corrosion cracking mechanism into the mid-1990s. [29] This section provides an

overview of relevant degradation mechanisms and steam generator tube rupture experience in the United States.

### 3.2.1 Recirculating Steam Generator Tube Degradation

In RSGs, tube degradation can occur in the following primary ways: wastage (wall-thinning), denting, pitting, fretting, wear, fatigue, primary side stress corrosion cracking (PWSCC), and outside diameter stress corrosion cracking (ODSCC). [30]

Figure 3.5 below is a schematic of these tube degradation mechanisms for RSGs.

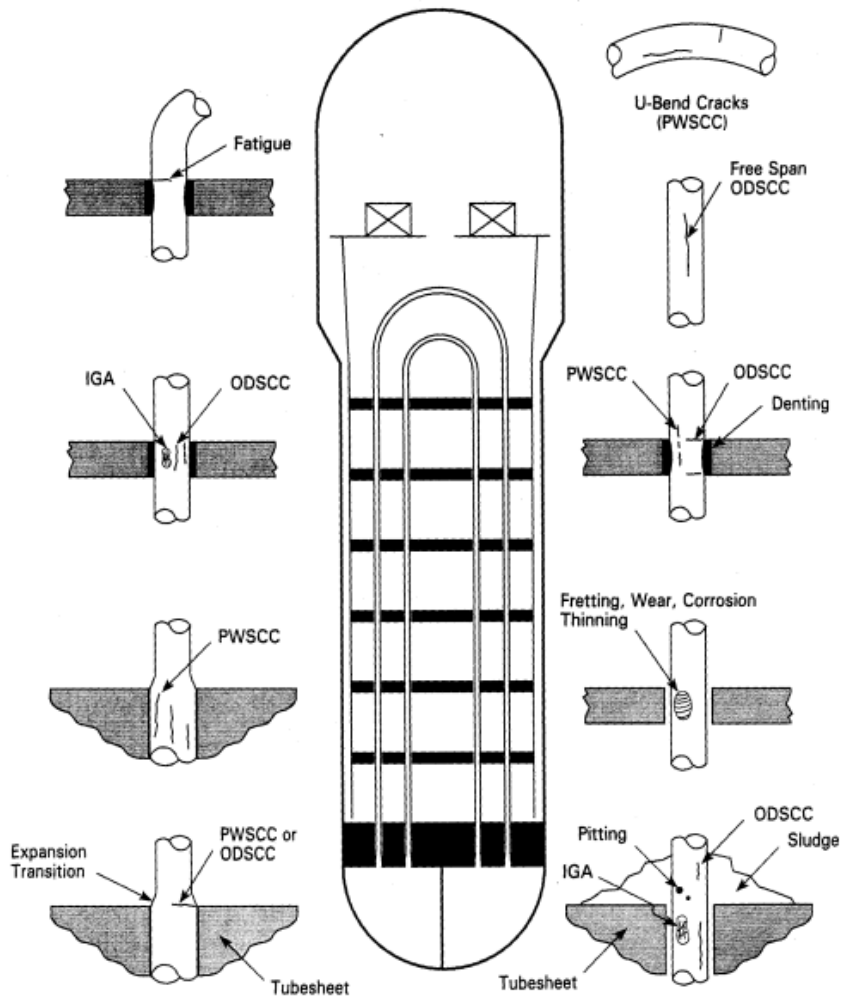


Figure 3.5 - Schematic of RSG tube degradation mechanisms [30]

### ***3.2.1.1 Wastage (Wall-thinning)***

Wastage was one of the primary degradation mechanisms in the 1970s when the secondary system used phosphate water as its feed-water. The system design allowed for the introduction of corrosion products and impurities to the steam generator causing sludge piles to settle on top of tube sheets. As a result, aggressive corrosion causes the outside walls of the tubes to deteriorate. When operators identified this critical issue, it was mostly corrected by changing the feed-water to all-volatile water treatment.[24]

### ***3.2.1.2 Denting***

Denting is a tube degradation mechanism occurring where the tube and the tube supports overlap. In early designs where the tube support plates were fabricated by drilling holes into carbon steel plates, rapid corrosion of carbon steel fills the annulus and squeezes the tube causing dents (usually on two sides). While denting does not directly cause tube failures, this degradation mechanism can increase susceptibility to PWSCC (See Section 3.2.1.5) or ODSCC (See Section 3.2.1.6).

### ***3.2.1.3 Pitting, Fretting and Wear***

When impurities such as chlorides, sulfur anions, and copper oxides are introduced to the steam generator on the secondary side system, RSGs may experience pitting from sludge pile regions on top of the tubesheets.

As a result of tube vibration induced by high flow rates at the U-bend areas of an RSG, fretting and wear occurs at the anti-vibration bars (See Figure 3.2). While the anti-vibration bars are installed to reduce vibration in the unsupported length of tube at the U-bend, they are also responsible for tube degradation. Other areas that experience wear are

at the tube support plates, where high flow rates cause the tube and tube support plates to interact negatively.

#### ***3.2.1.4 Fatigue***

Tube ruptures have been experienced due to fatigue degradation causing significant primary-to-secondary leaks. This form of degradation has occurred at the top tube support plate as a result of high frequency flow-induced vibration caused by cross flows at the U-bend area. In some cases, fatigue susceptibility increases due to a lack of anti-vibration bars or a large clearance between the tube and anti-vibration bars. Additionally, corrosion fatigue can occur if corrosion occurs between the tube and tube support plates.

#### ***3.2.1.5 Primary Water Stress Corrosion Cracking***

Since the 1980s [29], primary stress corrosion cracking (PWSCC) has been an on-going tube degradation mechanism. The mechanism is defined as cracking on the primary side (or inside) of the tube as a result of stress corrosion cracking. PWSCC is found in three locations of an RSG. Firstly, PWSCC occurs in the transition region in the tubesheet, where the tube is mechanically sealed to the tubesheet. At this location, the tubes experience high residual stresses due to the mechanical expansion techniques. The second location that experiences PWSCC is at the U-bends, where residual stresses are induced during the fabrication process by bending. Finally, PWSCC is seen at the tube support plates intersection where denting induces high residual stresses. Spanning across three different locations, this degradation mechanism is still a concern in the nuclear industry. PWSCC in Alloy 600 steam generator tubes is further explored in Section 3.4.

### **3.2.1.6 Outside Diameter Stress Corrosion Cracking**

Outside diameter stress corrosion cracking (ODSCC) has also been a continuing tube degradation mechanism since the early 1980s. As with PWSCC, ODSCC has occurred in multiple locations within an RSG including: in the tubesheet crevices, at the tube to tube support plate intersections, under sludge piles and sometimes in the free-span. This type of cracking is involved with the impurities of the secondary side feed-water (all-volatile water treatment) and also residual stresses in the tube due to operation or fabrication. ODSCC is also a tube degradation mechanism that is still a growing concern for plant operators.

### **3.2.2 Once-Through Steam Generator Tube Degradation**

The only main difference between OTSGs and RSGs is that the RSGs utilize U-bend tubes in the heat exchange process whereas OTSGs utilize straight tubes that require all the heat to be transferred as the primary coolant passes the steam generator once in a single direction. The only supplier for OTSGs is Babcock and Wilcox. Since the OTSGs are designed and manufactured slightly differently than RSGs, some of the tube degradation locations are different. Some tube degradation locations include: upper tubesheet crevice cracking, primary side cracking, upper span lane region circumferential cracking, upper tube support plate fretting and wear, and tube support plate erosion. Figure 3.6 is a schematic of these tube degradation mechanisms for OTSGs.

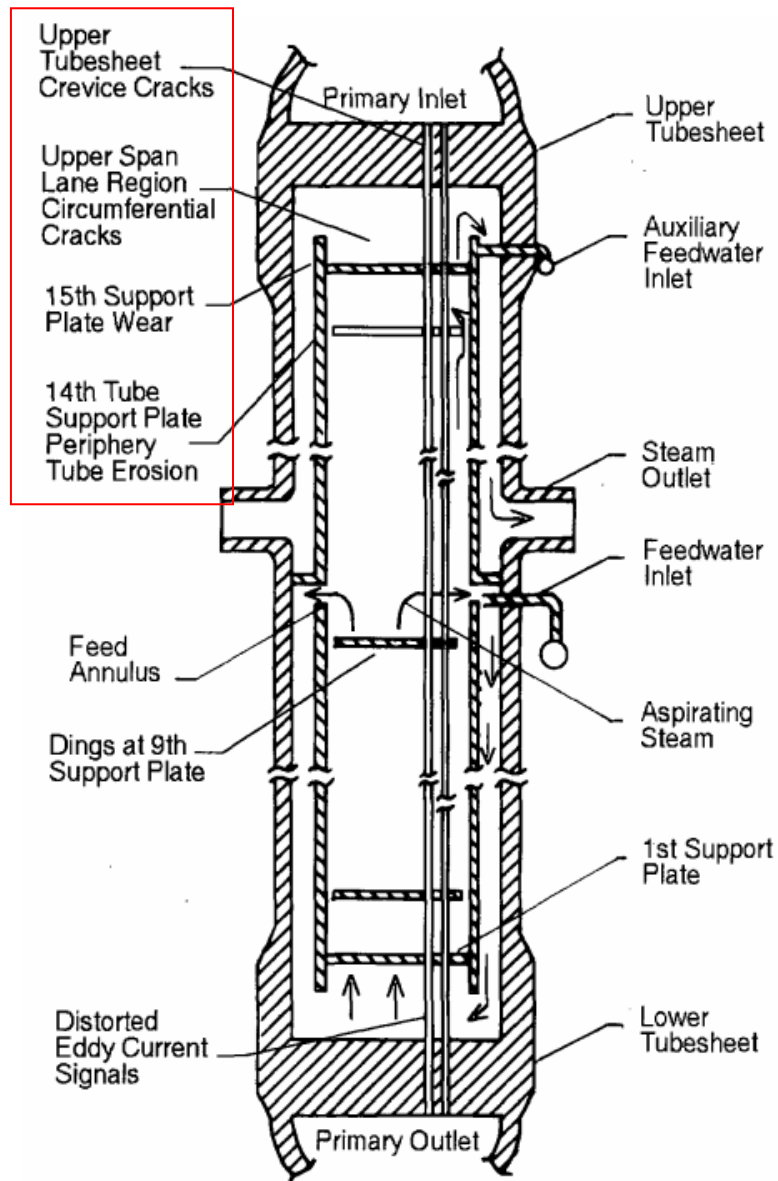


Figure 3.6 - Schematic of tube degradation mechanisms in OTSGs [24]

### 3.2.2.1 Upper Tubesheet Crevice Cracks + Primary Side Cracking

Power plants have experienced upper tubesheet crevice cracks due to sulfur attacking. Since all OTSG tubes are sensitized, they are all susceptible to sulfur attacks. In the same general area, sulfur attacks are also proposed to be responsible for tube degradation on the primary side of the tube transition regions.

### **3.2.2.2 Upper Span Circumferential Cracking**

Corrosion fatigue has been seen to occur in the upper span of the steam generator at the top tube support plate and at the bottom of the upper tubesheet causing circumferential cracking. High velocities of steam along with the concentration of impurities seem to be culprit for this cracking mechanism at this location. As a result of fatigue, fretting and wear between the tubes and the tube support plates are also degradation mechanisms seen in this area.

### **3.2.2.3 Tube Support Plate Erosion**

While the exact degradation mechanism for erosion-corrosion around the 14<sup>th</sup> tube support plate is not understood fully, operators have postulated that the degradation is related to the concentration of unvaporized water and solid corrosion products flowing through the gaps.

## **3.3 US Experience with Steam Generator Tube Ruptures**

Even though there are many known tube degradation mechanisms and affected locations, the United States has only experienced a couple steam generator tube ruptures (SGTRs) that have attributed to a significant loss of coolant.[31] This section explores the definition of steam generator tube rupture and the four most recent SGTRs.

According to the U.S. Nuclear Regulatory Commission[31], a SGTR – Loss of Coolant 1 (LOCA 1) occurs when a steam generator tube crack experiences a primary-to-secondary leak rate that is greater than a specified rate or when there is significant mechanical damage to the steam generator tube (causing a very high leak rate). This threshold leak rate varies depending on the steam generators specifications and operating conditions. In a report by the NRC [31], a SGTR – LOCA 1 is defined as steam generator



leak rates greater than 100 gpm. In some cases, a SGTR event is defined by the NRC as a primary-to-secondary side leak exceeding the normal charging pump capacity of the primary system. [32]

As such, NRC reported the following four SGTR: LOCA 1 occurrences from 1987 to present day: North Anna in 1987, McGuire in 1989, Palo Verde in 1993 and Indian Point in 2000. Thus, the frequency of steam generator tube ruptures is calculated using historical data. More specifically, NRC reported [31] a SGTR: LOCA 1 frequency per calendar year at the year 2002 mark by dividing the number of SGTRs by the effective operating calendar years across all of the steam generators. Since the report assessed four SGTRs between 1987 and 2002, the researchers estimated 1,133 total calendar years of reactor operation. Thus,  $4/1,133$  is approximately  $3.5 \times 10^{-3}$  steam generator tube ruptures per calendar year.

On July 15, 1987, a steam generator tube ruptured in the 'C' steam generator due to high cycle fatigue and denting at the uppermost tube support plate [33]. After the steam generator was brought down from operation, the unit operators calculated that the leak rate exceeded 100 gpd 19 hours prior to the rupture and over 500 gpd approximately six hours before rupture. The source of the mechanical loading was believed to be the combination of a high mean stress level induced by denting and alternating stress caused by flow-induced vibration in the U-bends.

On March 7, 1989, a steam generator tube ruptured due to axially oriented stress corrosion cracking. Prior to the rupture, unit operators estimated a leak rate of 15 gpd, which was insignificant as compared to the technical specifications performance limit of 500 gpd.

On March 14, 1993, a steam generator tube ruptured due to outside diameter stress corrosion cracking causing a primary-to-secondary leak of approximately 240 gpm.

### **3.4 Further Analysis on PWSCC in Steam Generator Tubes**

Since this research has a focus on primary water stress corrosion cracking in Alloy 600 steam generator tubes, the phenomenon is further explored in this section. As described briefly in Section 3.2.1.5, PWSCC as a tube degradation mechanism has been an ongoing concern for steam generator integrity due to its multiple locations of attack and the frequency of attacks. Moreover, this section will only focus on RSGs since it has been reported that PWSCC primarily occurs in Westinghouse-type steam generators (OTSGs were only manufactured by Babcock & Wilcox). [24]

#### **3.4.1 PWSCC Locations and Orientations**

Since there are a number of variations to the RSG, different cracking locations and orientations have been reported. The main locations for PWSCC are at the expansion transition regions, at the tube to tube support plate intersections, and at U-Bends. Figure 3.7 provides an overview of these cracking locations.

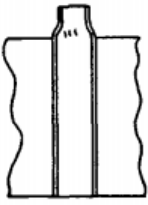
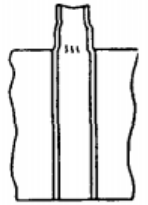
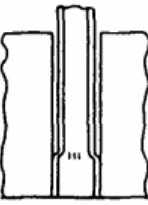
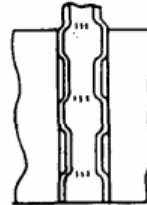
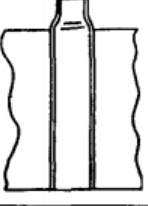
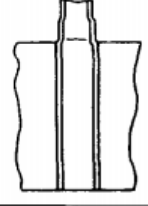
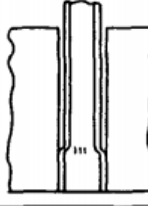
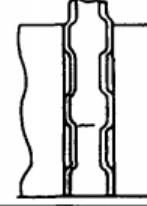
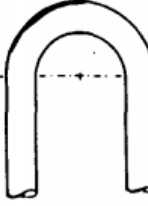
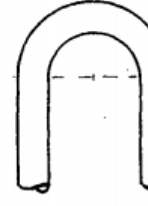
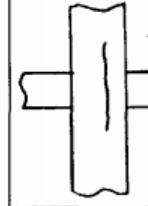
Location	Expansion Transitions—Longitudinal PWSCC			
	Full Depth w/o DAM	Full Depth With DAM	Part Depth	Intermittent
Sketch				
Location	Expansion Transitions—Circumferential PWSCC			
	Full Depth w/o DAM	Full Depth With DAM	Part Depth	Intermittent
Sketch				
Location	U-Bends		Tube Support Plates	
	Apex	Opposite Transition	Axial PWSCC	
Sketch				

Figure 3.7 - Overview of PWSCC cracking locations and orientations [24]

### 3.4.1.1 Expansion Transitions

On the primary side of the steam generator, the tubes are mechanically secured to the tubesheet by a number of expansion techniques, all of which induce high residual stresses. Originally, tubes were expanded only a short length at the bottom of the tubesheet, leaving a crevice for potential ODSCC. However, the partial-depth expansion also provided protection for the tubes in the case of circumferential rupturing since part of the tube resides in the tubesheet. In the early 1970s, designers began to shift from partial-depth expansion to full-depth expansion. Expansion techniques used in primary water reactors include: roll expansion, kiss-rolling, explosive expansion and hydraulic

expansion. It has been accepted that the roll expansion technique produces the highest residual stresses within the tubes as compared to the other expansion techniques.

Nevertheless, PWSCC has been observed for all expansion techniques.

As shown in Figure 3.7, cracking in the expansion transition region can occur longitudinally (axially) or circumferentially. Longitudinal cracks tend to line up in a parallel pattern around the circumference of the transition region. In some cases, the axial cracks assume a slightly curved orientation. As expected in this region, the cracks propagation rate decreases as the crack grows towards the non-expanded sections of the tube with lower mean level stresses. Circumferential cracks have the potential to grow through-wall 360° of the tube circumference causing dangerous tube ruptures. Due to the high pressures on the primary side, a circumferential 360° rupture may damage nearby tubes caused by whipping. However, it is fortunate that historical evidence has shown that circumferential cracking occurs much less often than longitudinal cracking in expansion regions.[24]

#### ***3.4.1.2 Tube Support Plate Interactions***

Axial cracking at tube support plate interactions begins by denting due to the build-up of corrosion products in the clearance between the tube and the tube support plate. The denting squeezes the tube symmetrically from both sides as shown in Figure 3.8 and effectively increases the residual stress on the tube at that location.

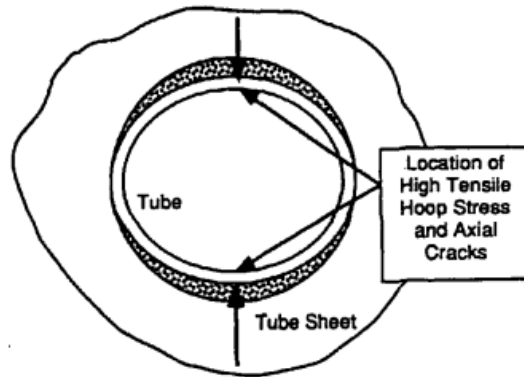


Figure 3.8 - PWSCC initiated by denting at tube support plate interactions [24]

### 3.4.1.3 U-Bends

Cracking at U-Bends can occur at the apex of the bend or at the U-Bend tangents (when the straight tube transitions into the curve). At the apex of the bends, there are already high residual stresses from the fabrication stage. However, this stress is further increased when denting occurs at the tube support plates causing the tube to pinch. Figure 3.9 provides a schematic diagram of this phenomenon. Aside from denting, apex cracking can also occur due to excessive ovality in Rows 1, 2 and 3 of steam generator tube bundles. The U-bends for these tubes have a very tight radius and thus the residual stresses are high.

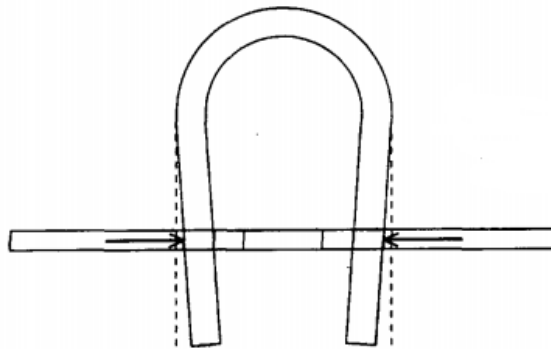


Figure 3.9 - Tube pinching due to denting at the tube support plate causing PWSCC at the U-Bend apex [24]

### 3.4.2 Overview of Applied and Residual Stresses

As mentioned, the total effective stress for PWSCC is the arithmetic sum of the operating stress and the residual stress. While the operating stresses remain constant between the three PWSCC locations, residual stresses in all three locations may be different. Also, since residual stress can be induced aside from initial manufacturing, these stresses are not necessarily constant even at specific locations. Table 3.3 shows a breakdown of the operating (pressure difference and thermal stresses) and approximate residual stresses for the affected regions.[24][34]

**Table 3.3 - Estimated operating and residual stress levels at affected locations**

<b>Location</b>	<b>Pressure Difference (axial/hoop) [ksi]</b>	<b>Thermal (axial/hoop) [ksi]</b>	<b>Residual (axial/hoop) [ksi]</b>
Rolled Expansion Transition	5/11	-7/-7	45-49/54-62
Tube Support Plate (w/o denting)	5/11	0/0	-1/-25
Tube Support Plate (with denting)	0/0	0/0	60/60
U-Bend Row 1	5/11	-4/-4	90/50-68
U-Bend Row 2	5/11	-4/-4	68/74

[1 ksi = 6.895 MPa]

As shown, operating stress due to primary-secondary side pressure differences are not substantial. However, residual stresses are observed to be magnitudes greater than operating stresses with the highest stresses in the U-Bends. Axial stresses and hoop stresses are generally responsible for circumferential and longitudinal (axial) cracking, respectively.

### 3.4.3 Other PWSCC Conditions in Alloy 600 Tubes

In Alloy 600 steam generator tubes, SCC propagates intergranularly in the direction perpendicular to the applied tensile stress. In operation, the protective oxide

film forms over the alloy surface, thus decreasing the corrosion of grains boundaries. However, when a tensile stress is induced on the material, the strain may break the film allowing the bulk primary water to come in direct contact with the bare surface. For the case of Alloy 600 steam generator tubes, SCC can initiate at pre-existing cracks caused by other mechanisms, surface discontinuities, or locations with inconsistent material composition. [24] After the crack has been initiated, the applied tensile stress maintains a crack opening that leads to accelerated dissolution or rupture. One known method for reducing the SCC susceptibility is to alter the tubes' microstructure by increasing the chromium carbide precipitation and decreasing the carbon content. Since PWSCC is primarily intergranular cracking, research has shown that increasing the grain size and the chromium carbide precipitation coverage along the grain boundaries through high temperature mill-annealing provides better resistance to SCC [35].

Historical operating experience [24] shows that PWSCC does not occur in Alloy 600 steam generator tubing if the total effective stress (operating applied + residual) is less than 35 ksi (240MPa). As shown in Table 3.3, normal operating stresses (due to pressure and thermal differentials) do not exceed this threshold and confirms that PWSCC occurs only at locations where residual stresses are induced.

Experience has also shown that temperature is a critical parameter in controlling PWSCC. Gorman et al. [36] has shown that PWSCC degradation in LTMA tubes increases with increasing temperature. Also the researchers proposed that temperature dependence on PWSCC propagation can be described by an Arrhenius relationship such that the activation energy for propagation is between 45 and 50 kcal/mol. Later, the range for propagation activation was revised to 25-30 kcal/mol after further laboratory testing.

## Chapter 4 Development of Empirical SCC Propagation Model

Stress corrosion crack propagation mechanisms and models have been proposed in research as described in Section 2.3.3 and Section 2.3.4. Some of them are theoretically derived from postulated cracking mechanisms for all scenarios of SCC such as the FRI model developed by T. Shoji and co-workers [4], while others have been developed semi-empirically for specific scenarios of SCC such as the model developed by Scott [5]. In a theoretically derived model as with the FRI model, there are a number of variables that alter the resultant predicted crack propagation rate depending on the SCC scenario. On the other hand, semi-empirically developed models have very few variables. In Scott's model, the only variable is the stress intensity factor (a function of the total effective stress and the crack length). All other values were parameters of the model as determined by experimental data. Coupled with experimental data, semi-empirical crack propagation models provide a balance between ease of use and mechanistic accuracy.

In this research, an existing empirical model has been extended to estimate the crack propagation rate for PWSCC of Alloy 600 with a focus on steam generator tubes. The existing model is extended to incorporate two other factors that also affect SCC propagation: pH and yield strength. This chapter describes the variables used in this model, their respective numerical relationships to the SCC propagation rate, and elaborates on the model formation process. Additionally, this chapter utilizes available crack propagation data for Alloy 600 steam generator tubes to estimate the model parameters using Bayesian estimation techniques in open source software called WinBUGS.



## 4.1 Base Empirical Model

The final proposed model begins with a base existing model as proposed by the J. Hicking et al. from the Electric Power Research Institute (EPRI) [20], known as the MRP model, originally developed for evaluation of thick-wall components fabricated from Alloy 600 material. The structure of this model is almost identical to that of Scott's [5] for steam generator tubes with the exception of the addition of a temperature relationship. The MRP model is explored in Section 2.3.4, but re-iterated here for convenience.

$$\dot{a} = \alpha \cdot \exp \left[ -\frac{Q}{R} \left( \frac{1}{T} - \frac{1}{T_{ref}} \right) \right] \cdot (K - K_{th})^\beta$$

where:  $\dot{a}$  – crack growth rate  
 $R$  – universal gas constant  
 $T_{ref}$  – reference temperature  
 $K_{th}$  – threshold SIF  
 $\beta$  – model parameter  
 $Q$  – activation energy for propagation  
 $T$  – operating temperature  
 $K$  – stress intensity factor (SIF)  
 $\alpha$  – crack growth amplitude parameter

As such, the MRP curve is used as a base empirical model, since it incorporates two factors affecting the crack propagation rate of SCC in Alloy 600 material: stress and temperature.

It has been accepted that the crack propagation of SCC can be represented by a power-law function where the dependent variable is the stress intensity factor. [9][24][5] The stress intensity factor is a general function defined by:

$$K = \sigma_{applied} \sqrt{\pi a}$$

where  $K$  is the stress intensity factor,  $\sigma_{applied}$  is the total effective stress on the material, and  $a$  is the crack length. As a result, since SCC propagation conditions require a constant applied tensile stress, the stress intensity factor increases as the crack depth

increases. This model also incorporates the threshold stress intensity factor required for SCC propagation. This value was determined to be  $9\text{MPa}\sqrt{\text{m}}$  for steam generator tubes by Scott [5], but can vary depending on the SCC scenario (e.g. steam generator tubes versus control rod drive mechanism nozzles).

Experience and research has demonstrated that temperature is a critical factor that negatively affects the SCC propagation of Alloy 600 materials. [36][20][3] The relationship is such that increasing the operating temperature increases the crack propagation rate and in turn decreases the time-to-failure. Gorman et. al [36] postulated that the temperature dependence on SCC follows an Arrhenius relationship as such:

$$\text{time} - \text{to} - \text{failure} \propto \exp\left(\frac{Q}{RT}\right)$$

The MRP adopts this well-known relationship and includes a  $T_{ref}$  constant for added flexibility in normalizing the model to a specified temperature.

Figure 4.1 shows a graph of SCC propagation rate versus  $1/T$  for 35% cold worked Alloy 600 tubing. [37] For this experiment, the activation energy,  $Q$ , is shown to be 124 kJ/mol.

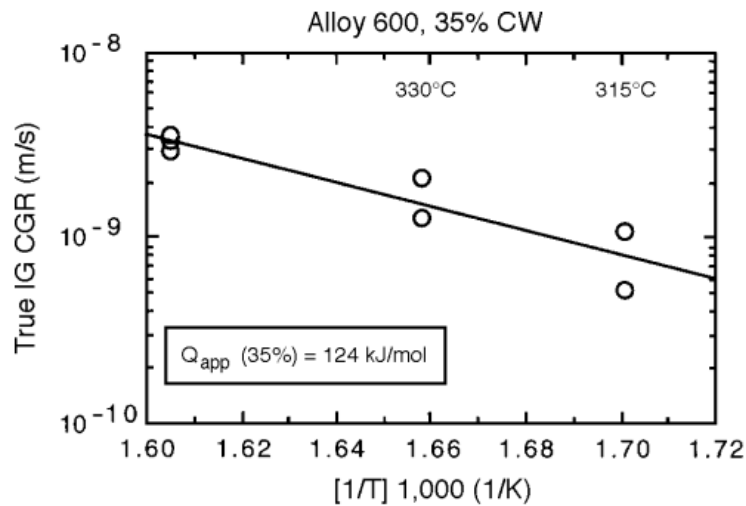


Figure 4.1 - CPR versus  $1/T$  graph [37]

## 4.2 Added Factors – pH and Yield Strength

While the MRP model accounts for the constant applied stress and temperature factors of SCC in Alloy 600, it does not incorporate factors such as pH and yield strength. Since SCC propagation occurs only in a corrosive environment, the bulk solution chemistry is very important in estimating the crack propagation rate. Among other bulk chemistry parameters, research [38] has shown that an increase or decrease of pH from the neutral value increases the crack propagation rate. Moreover, a power-law dependency has been proposed to be the numerical relationship corresponding to the crack propagation rate. The relationship is described as follows:

$$CPR \propto [pH]^\beta$$

where  $CPR$  is the crack propagation rate,  $pH$  is the pH of the bulk solution and  $\beta$  is the relationship parameter. Using available experimental data [38], Figure 4.2 shows a graph of crack propagation rate versus pH for different K values.

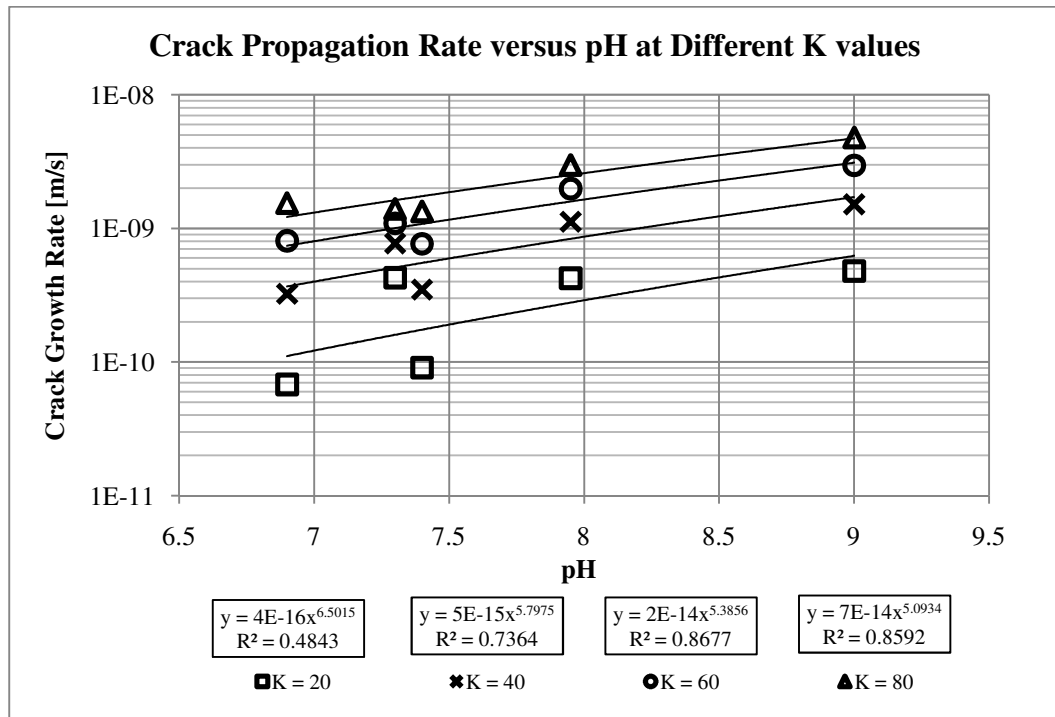


Figure 4.2 – Crack propagation rate as a function of pH at different K values

The power relationship between the crack propagation rate and the pH of the bulk environment is assessed in Figure 4.2. The fit of the relationship increases with increase in the stress intensity factor,  $K$ . For  $K = 20 \text{ MPa}\sqrt{\text{m}}$ , the R-value for the power-law trend line is 0.4843. For  $K = 40 \text{ MPa}\sqrt{\text{m}}$ , the R-value is 0.7364 indicating a better fit than at  $K = 20 \text{ MPa}\sqrt{\text{m}}$ . For  $K = 60$  and  $80 \text{ MPa}\sqrt{\text{m}}$ , the R-values are 0.8677 and 0.8592, respectively. Therefore, assuming that an R-value of 0.70 indicates a fair fit, the power-law relationship for pH can only be applied to Stage II of SCC propagation. The R-value of 0.4843 at  $K = 20 \text{ MPa}\sqrt{\text{m}}$  does not justify the use of this pH relationship. However, these observations align with the SCC phenomenon, which proposes that Stage I is driven primarily by the applied stress and Stage II is driven primarily by the corrosive environment (See Section 2.1).

Since material microstructure can affect the SCC propagation in Alloy 600, the other factor incorporated into this model is yield strength. Yield strength is the stress at which a material begins to deform plastically. This value is not only specific to the type and composition of a material, but also its microstructure. For instance, it is known that work-hardening a material reduces its ductility, increases its toughness and also increases its yield strength. As such, there is a linear relationship between the amount of cold work performed and the yield strength. Table 4.1 shows the yield strength of Alloy 600 at different percentages of cold working calculated from hardness as reported by Rebak et al. [37] Figure 4.3 shows an R-value of 0.9985 for the linear relationship.

**Table 4.1 - Yield strengths for Alloy 600 at various cold work percentages [37]**

<b>Specimen</b>	<b>Vickers Hardness</b>	<b>Yield Strength [MPa]</b>
As Received	195	359
16% Cold Work	255	620
35% Cold Work	315	976

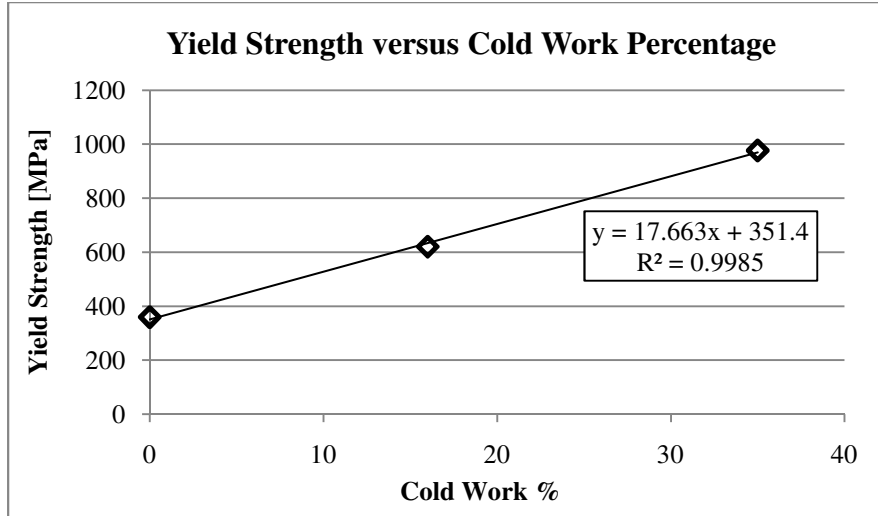


Figure 4.3 - Yield Strength as a function of Cold Work Percentage

Thus, yield strength is incorporated into the final model in order to better characterize the Alloy 600 microstructure. Rebak et al. [37] and Speidel et al. [39] proposed a power-law relationship to describe the dependence of percent of cold work and yield strength to crack propagation rate. As expected, increasing the cold work and thus the yield strength of a material increases the crack propagation rate. The relationship used is as follows:

$$CPR \propto [\sigma_{ys}]^m$$

where  $CPR$  is the crack propagation rate,  $\sigma_{ys}$  is the material yield strength, and  $m$  is the power relationship parameter. This research uses the yield strength as a variable instead of the cold work percentage since the percentage of cold work can sometimes be arbitrary. On the other hand, yield strength can be mathematically calculated by hardness values. By fitting a power-law relationship into available SCC data [37], the dependency can be quantified. Figure 4.4 shows a graph of the crack propagation rate versus yield strength for Alloy 600 exposed to primary water for temperatures 330°C and 350°C.

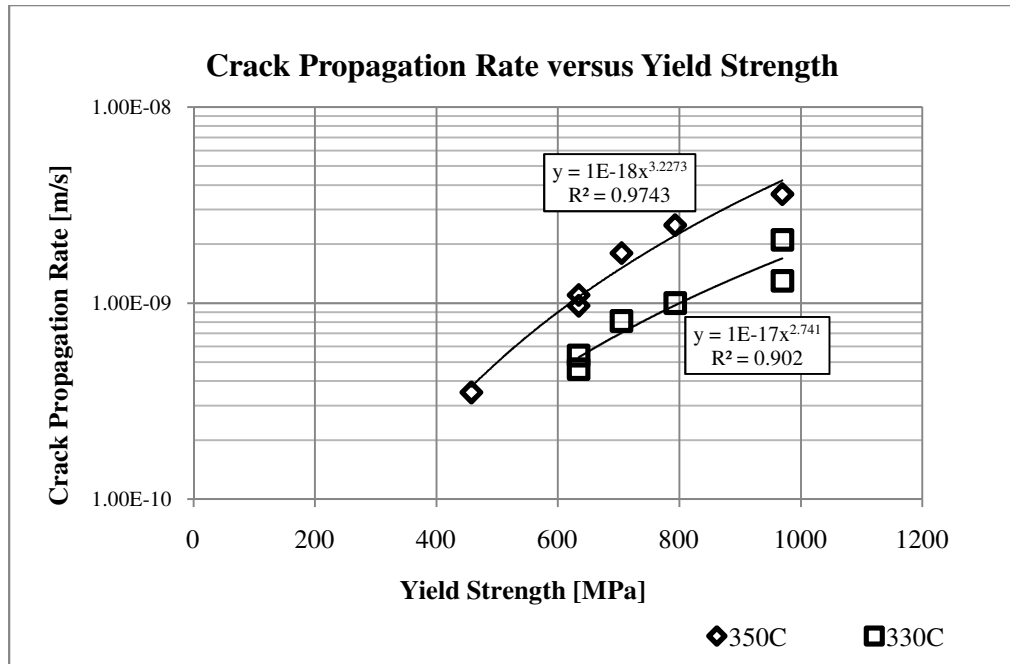


Figure 4.4 – Crack propagation rate as a function of yield strength

The R-values for the power-law relationship for yield strength are 0.902 and 0.9743 for 330°C and 350°C respectively. As such, the power-law relationship is applied to both the entire SCC propagation stage.

### 4.3 Final Proposed Model

The formation of the final model involves superimposing the numerical relationships (Section 4.2) to the base empirical model developed by EPRI. Table 4.2 below breaks down the factors that are incorporated in this final proposed model and their respective numerical relationships.

**Table 4.2 - Breakdown of incorporated SCC factors in final model**

<b>Incorporated SCC Factor</b>	<b>Relationship</b>	<b>Numerical Relationship</b>
Applied + Residual Stresses	Power Law	$[K - K_{th}]^\beta$
Environment pH	Power Law	$[pH]^\beta$
Environment Temperature	Arrhenius Relationship	$exp \left[ -\frac{Q}{R} \left( \frac{1}{T} - \frac{1}{T_{ref}} \right) \right]$
Material Cold Work/Yield Stress	Power Law	$[\sigma_{ys}]^m$

By combining all of the factors, the general equations for Stage I and II crack propagation rate become:

$$CPR_I = C \cdot exp \left[ \frac{Q}{R} \left( \frac{1}{T} - \frac{1}{T_{ref}} \right) \right] \cdot [\sigma_{ys}]^m \cdot [K - K_{th}]^n$$

$$CPR_{II} = C \cdot exp \left[ \frac{Q}{R} \left( \frac{1}{T} - \frac{1}{T_{ref}} \right) \right] \cdot [pH]^\beta \cdot [\sigma_{ys}]^m \cdot [K - K_{th}]^n$$

where  $C$  is a constant. Note that the pH variable is omitted from  $CGR_I$  due to the lack of dependency. Also, it is noted that the model parameters from the existing equation are translated to  $C$  and  $n$  rather than  $\alpha$  and  $\beta$ .

As shown in Figure 2.3 and described in Section 2.2, the SCC propagation stage is split up in three separate stages: Stage I, Stage II and Stage III. Since Stage III is very rapid in comparison to Stages I and II, it is assumed to be negligible and is not modeled. Stage I appears to be much more dependent on the stress intensity factor while Stage II is virtually independent of the stress intensity factor. Theoretically, Stage I propagation is

driven primarily by stress intensity and Stage II propagation is primarily driven by environmental stressors. However, these ideal conditions are not portrayed in experimental and industry data. [40] As such, the model parameters for Stages I and II will be unique. In order to achieve smooth transition from Stage I to Stage II equations, the following final model is proposed to be:

$$CPR = \begin{cases} CPR_I & \text{for } K < K_{trs} \\ CPR_I(1 - x) + CPR_{II}(x) & \text{for } K_{trs} \leq K < K_{tre} \\ CPR_{II} & \text{for } K \geq K_{tre} \end{cases}$$

where:

$$CPR_I = C_I \cdot \exp \left[ \frac{Q}{R} \left( \frac{1}{T} - \frac{1}{T_{ref}} \right) \right] \cdot [\sigma_{ys}]^{m_I} \cdot [K - K_{th}]^{n_I}$$

$$CPR_{II} = C_{II} \cdot \exp \left[ \frac{Q}{R} \left( \frac{1}{T} - \frac{1}{T_{ref}} \right) \right] \cdot [pH]^{\beta_{II}} \cdot [\sigma_{ys}]^{m_{II}} \cdot [K - K_{th}]^{n_{II}}$$

$K$  – stress intensity factor (SIF)

$K_{trs}$  – approximate SIF at the beginning of the Stage I to Stage II transition

$K_{tre}$  – approximate SIF at the end of the Stage I to Stage II transition

$CPR$  – linearly combined crack propagation rate

$CPR_I$  – crack propagation rate for Stage I crack propagation

$CPR_{II}$  – crack propagation rate for Stage II crack propagation

$x$  – transition ratio defined by  $(K - K_{trs}) / (K_{tre} - K_{trs})$

and

$Q$  – activation energy (130 kJ/mol[20][41])

$C_I, C_{II}$  – model constants

$R$  – universal gas constant (8.314E-3 kJ/mol-K)

$\beta_{II}$  – parameter for pH

$T$  – operating temperature

$m_I, m_{II}$  – parameters for Y.S.

$T_{ref}$  – reference temperature (588 K)

$n_I, n_{II}$  – parameters for SIF

pH – pH of the bulk environment

$\sigma_{ys}$  – material yield strength



$K_{th}$  – threshold SIF (9MPa $\sqrt{m}$  [5])

Variables  $K_{trs}$  and  $K_{tre}$  are defined as approximate stress intensity factors at the beginning of the Stage I to II transition and approximate stress intensity factors at the end of the Stage I to II transition, respectively. When the stress intensity is less than  $K_{trs}$ , the crack propagation rate is in Stage I and is described by  $CGR_I$ . When the stress intensity is greater than  $K_{tre}$ , the crack propagation rate is in Stage II and is described by  $CGR_{II}$ . In the defined transition region, between  $K_{trs}$  and  $K_{tre}$ , the crack propagation rate is defined by the linear combination of  $CGR_I$  and  $CGR_{II}$ .

#### 4.4 Model Parameter Estimation Using Experimental Data

Model parameters  $\{C^*, n^*, m^*, \beta^*\}$  are estimated by fitting the model into the appropriate experimental crack propagation data. Variables  $K_{trs}$  and  $K_{tre}$  are defined by the end-user via assessment of the data.

##### 4.4.1 Bayesian Regression Analysis

One method for estimating the model parameters with experimental data is the use of Bayesian techniques with Markov Chains-Monte Carlo sampling algorithms. By definition, Bayesian analysis is a statistical method that makes inference on unknown values of interest by combining prior beliefs of the unknown values of interest and concrete observed information regarding the values. The resultant values are called the posterior. As such, Bayesian techniques provide an estimation of the model parameters with uncertainty in the form of a joint probability density function, which also preserves the shape of the data scatter. The posterior distribution for the model parameters given

$\underline{\theta} = \{C, n, m, b, s\}$  and  $Data = \{CPR_i, K_i, pH_i, T_i, \sigma_{ys_i}\}$  is:

$$\pi(\underline{\theta}|Data) = \frac{L(Data|\underline{\theta})\pi_o(\underline{\theta})}{\int L(Data|\underline{\theta})\pi_o(\underline{\theta})d\underline{\theta}}$$

where  $\pi(\underline{\theta}|Data)$  is the posterior distribution,  $L(Data|\underline{\theta})$  is the likelihood function for regression,  $\pi_o(\underline{\theta})$  is the prior beliefs of the model parameters.

In order to estimate the model parameters based on experimental data, Bayesian regression assumes that the likelihood function is used to describe the distribution of model error. More specifically, if the difference between the observed data and the best fitted model (with the most appropriate model parameters) is a random variable, the distribution of this random variable can be described by the likelihood function. In this situation, the likelihood function is assumed to be normal. Thus, this assumes that for the most appropriate parameters, the error is normally distributed with a mean value of zero. The standard deviation of this distribution is estimated with the model parameters. For the developed model and a set of experimental data, the normal likelihood can be defined by:

$$L(Data|\underline{\theta}) = \prod_{i=1}^N \frac{1}{s\sqrt{2\pi}} e^{-\frac{1}{2}\left(\frac{CPR_{exp}[i] - CPR_{calc}[i, \underline{\theta}]}{s}\right)^2}$$

where  $N$  is the total number of data points,  $s$  is the standard deviation of the error,  $CPR_{exp}[i]$  is the  $i$ -th experimental value for crack propagation rate, and  $CPR_{calc}[i, \underline{\theta}]$  is the  $i$ -th calculated value for crack propagation rate given the parameter set  $\underline{\theta}$ .

The joint posterior distribution of the parameters can be numerically solved using open source software called WinBUGS. This software utilizes Bayesian techniques with Markov chain Monte Carlo sampling methods to iterate and numerically yield the joint

distribution. More information about the WinBUGS Open Source Software can be found in Cowles [42].

#### 4.4.2 Estimating Model Parameters using Alloy 600 Data

The focus on this research is to model stress corrosion cracking of Alloy 600 material in primary water conditions. As such, experimental data available [40][43][44] is collected and used as observed evidence in the Bayesian regression analysis process to estimate the model parameters. Figure 4.5 presents experimental data for SCC of Alloy 600 steam generator tubes in primary water conditions.

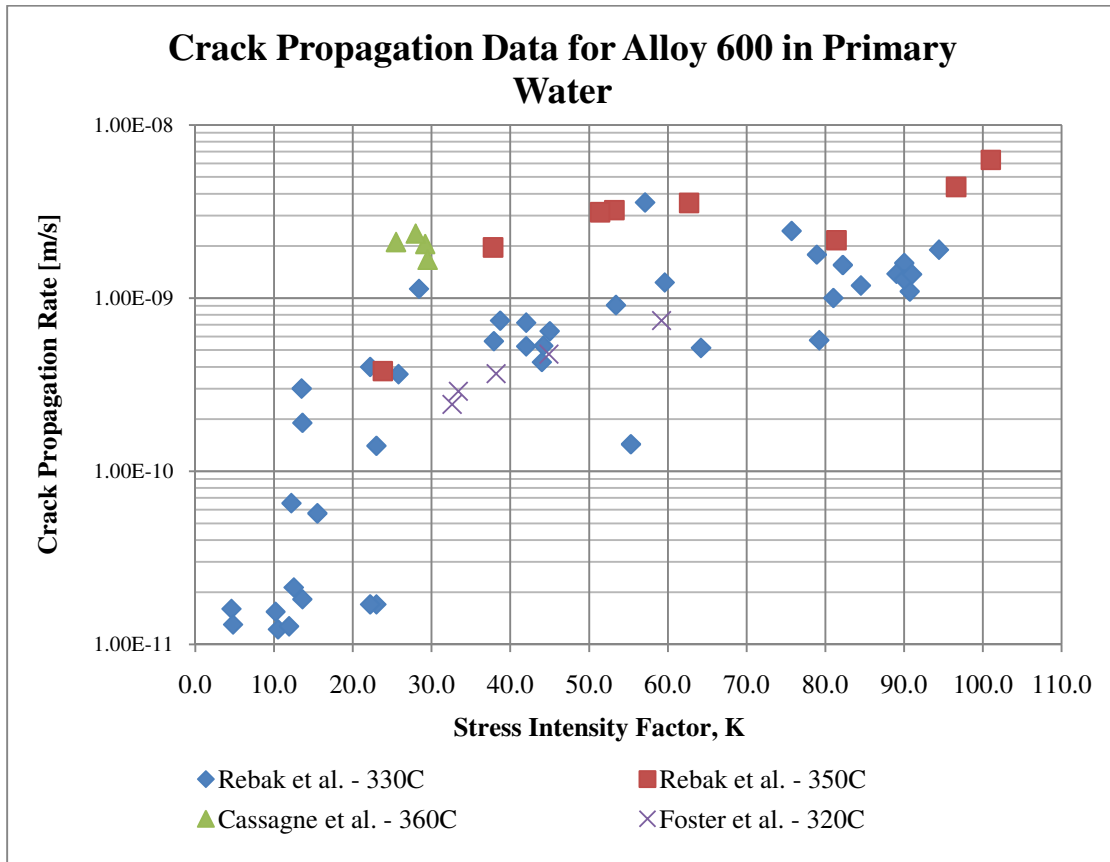


Figure 4.5 - Crack propagation data for Alloy 600 in primary water

Since the final model considers pH and yield stress in addition to the stress intensity and temperature, the specific environmental and material conditions for each set of data are

summarized in the Table 4.3. The entire set of data used for parameter estimation can be found in Appendix A.

**Table 4.3 - Material and Environmental Conditions for experimental data used**

<b>Source</b>	<b>Temp [°C]</b>	<b>pH</b>	<b><math>\sigma_{ys}</math>[MPa]</b>	<b>Cold Work [%]</b>
Rebak et al. [40]	330 – 350	5.2 – 9	389	1.5
Cassange et al. [43]	360	7.3	443	5
Foster et al. [44]	320	7.3	359	0

Collectively, the crack propagation rate is bounded by  $1 \times 10^{-11}$  and  $1 \times 10^{-8}$  meters per second. As shown, the crack propagation behavior increases rapidly with little change in stress intensity factor in Stage I. The data begins to flatten out as it transitions to Stage II at approximately 25 MPa $\sqrt{m}$ . Thus, the data is agreeable with the postulated SCC propagation phenomenology.

A prior distribution for the model parameters is also required to execute Bayesian regression analysis. Since no prior information is available for the model parameters, non-informative uniform priors are used for the regression analysis. Table 4.4 summarizes the uniform priors used in the parameter estimation of Stage I propagation.

**Table 4.4 - Uniform Priors for Stage I model parameters**

<b>Parameter</b>	<b>Lower Bound</b>	<b>Upper Bound</b>
$C_I$	0	5E-11
$n_I$	0	10
$m_I$	0	10
$s_I$	0	1E-7

The bounds for  $n_I$  and  $m_I$  are defined from 0 to 10 because it has been shown that an increase of stress and yield strength induces an increase in crack propagation rate. The lower bound for  $s_I$  is zero because the standard deviation cannot be negative. The upper

bound for  $s_I$  is 1E-7 in order to make no assumptions about the standard deviation. The bounds for  $C_I$  were estimated by back-calculating from the experimental data. Table 4.5 summarizes the uniform priors used in parameter estimation of Stage II propagation.

**Table 4.5 - Uniform Priors for Stage II model parameters**

<b>Parameter</b>	<b>Lower Bound</b>	<b>Upper Bound</b>
$C_{II}$	0	5E-11
$n_{II}$	0	10
$m_{II}$	0	10
$\beta_{II}$	0	10
$s_{II}$	0	1E-7

The bounds for the uniform priors for  $C_{II}$ ,  $n_{II}$ ,  $m_{II}$ , and  $s_{II}$  are have the same rationale as the uniform priors for  $C_I$ ,  $n_I$ ,  $m_I$ , and  $s_I$ . Since pH has a direct relationship to the crack propagation rate, the bounds for  $\beta_{II}$  are also 0 and 10.

As explained in Section 4.3, two sets of model parameters must be estimated: one set for Stage I crack propagation and another for Stage II. By visually assessing Figure 4.5, it is assumed that the transition region between Stage I and Stage II begins at  $K = 20\text{MPa}\sqrt{\text{m}}$  and ends at  $K = 30\text{MPa}\sqrt{\text{m}}$ . In order to develop a smooth and accurate transition region, the specific set of data used to estimate Stage I and II model parameters ranges 9 – 30  $\text{MPa}\sqrt{\text{m}}$  and 20 – 110 $\text{MPa}\sqrt{\text{m}}$ , respectively. Note that the Stage I data span across to the end of the transition region and the Stage II data spans across to the beginning.

#### **4.4.3 Model Parameter Set Results**

Using an open source Bayesian analysis software package called WinBUGS, the two sets of model parameters are estimated by Bayesian regression with MCMC sampling. The WinBUGS model coding can be found in Appendix B.

The posterior joint distribution can be represented by marginal distributions for each of the model parameters. The posterior marginal distributions for Stage I and Stage II are shown graphically in Figure 4.6 and Figure 4.7, respectively. Table 4.6 summarizes the model parameter distributions for Stage I and Stage II.

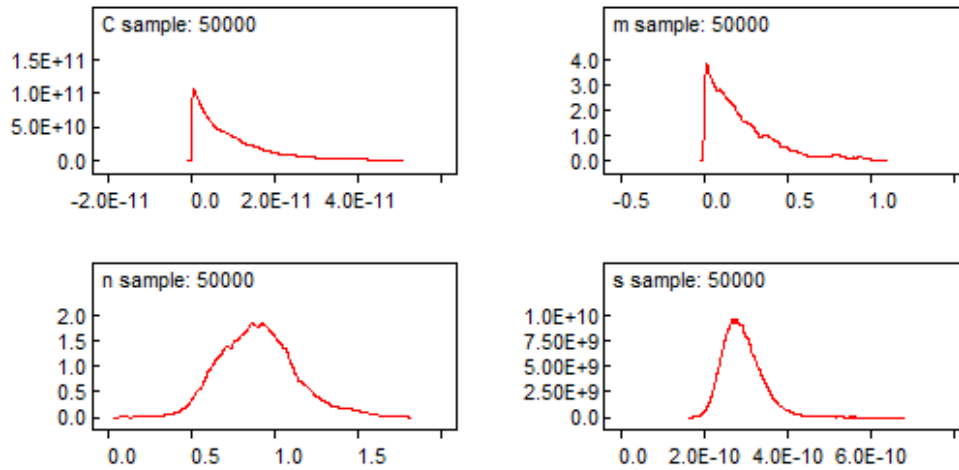


Figure 4.6 – Marginal distributions for Stage I model parameters and s.d.

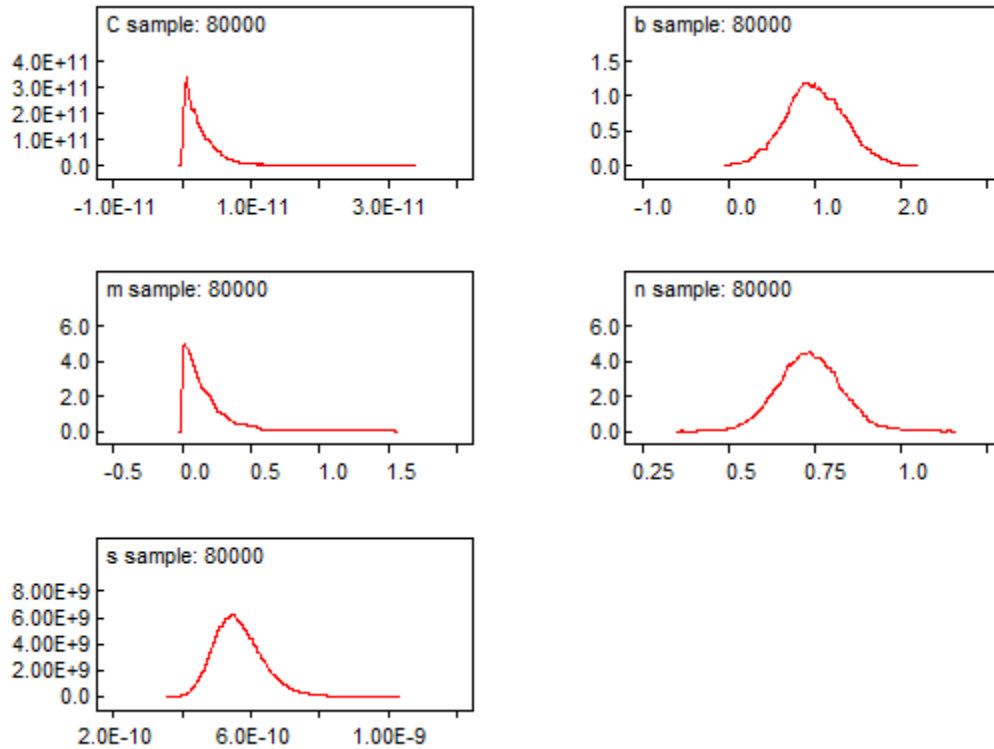


Figure 4.7 - Marginal distributions for Stage II model parameters and s.d.

**Table 4.6 - Summary of Stage I and Stage II model parameter distributions**

<b>Stage I Parameter</b>	<b>Mean</b>	<b>Standard Deviation</b>	<b>2.5%</b>	<b>97.5%</b>
$C_I$	9.703E-12	1.005E-10	1.033E-13	3.772E-11
$n_I$	0.8982	0.2268	0.5031	1.418
$m_I$	0.2286	0.2079	0.006021	0.8144
$s_I$	2.91E-10	1.079E-10	2.183E-10	3.932E-10
<b>Stage II Parameter</b>	<b>Mean</b>	<b>Standard Deviation</b>	<b>2.5%</b>	<b>97.5%</b>
$C_{II}$	2.858E-12	1.0E-10	1.505E-14	1.191E-11
$n_{II}$	0.736	0.09146	0.5595	0.9186
$m_{II}$	0.1836	0.2253	0.004685	0.9491
$\beta_{II}$	1.008	0.3418	0.3466	1.696
$s_{II}$	5.636E-10	1.216E-10	4.477E-10	7.18E-10

Using the estimated model parameters and the final proposed model, the calculated crack propagation rates with upper (97.5%) and lower (2.5%) are compared against the observed data. The model is determined to fit well into the data given the estimated model parameters and their uncertainties.

Figure 4.8 shows observed propagation rate data compared to the model for specimens with yield strength of 389MPa at 330°C in primary water with pH 7.3. This represents a typical primary water environment for steam generators.

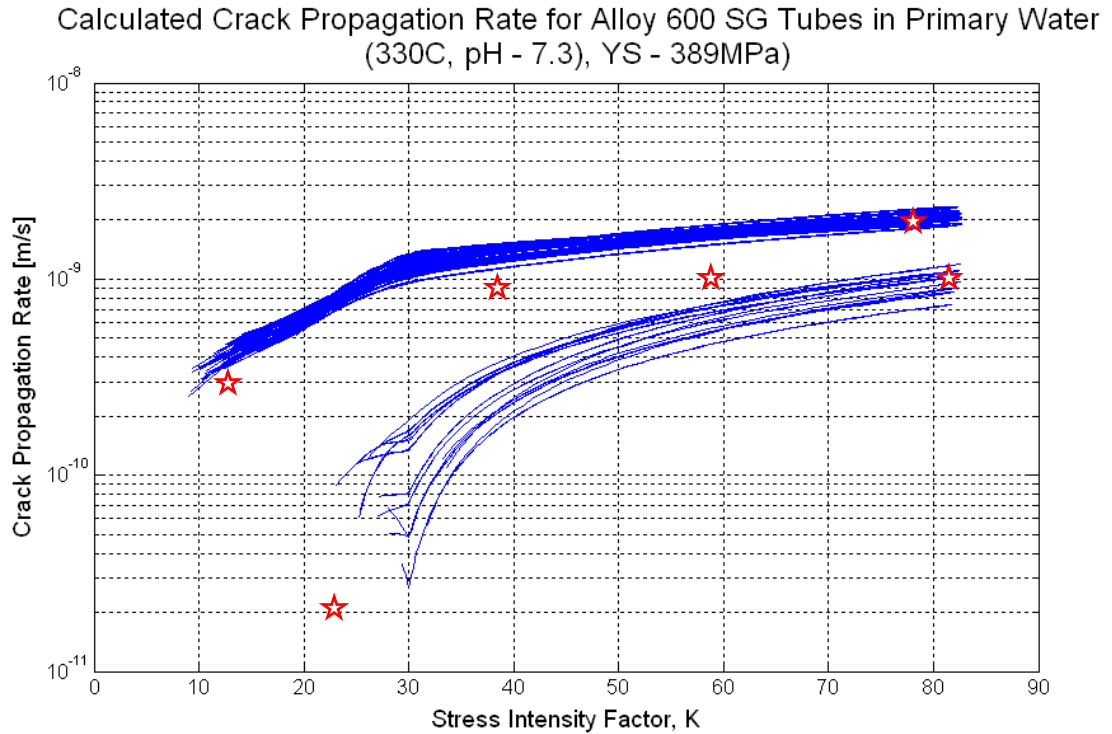


**Figure 4.8 – Calculated crack propagation rate for PWSCC of Alloy 600 in (pH - 7.3,  $\sigma_{ys}$  = 389MPa)**

The model has good correlation with the experimental data as shown in the figure above where the blue lines are each one standard deviation from the mean calculated crack propagation rate. In order to retain the shape and magnitude of the posterior model parameter distributions, the raw data for the marginal distributions can be used in simulations. In this particular estimation, 50,000 and 80,000 iterations were needed to obtain smooth marginal distributions for Stage I and Stage II.



## **Chapter 5 Simulating PWSCC of Alloy 600 Steam Generator**

### **Tubes**

In this research, stress corrosion crack propagation of Alloy 600 steam generator tubes in primary water environments is simulated using the model proposed in Section 4.3. Specifically, the simulation process provides a distribution of the time required for a crack to propagate 100% through the thickness of the steam generator tube. It is important to note that a 100% through-wall extent across the thickness of the tube is not classified as a "steam generator tube rupture". In this chapter, a 100% through-wall crack will be considered a "failure". The failure criterion is further explained in Section 5.3. This chapter describes the simulation process, initial assumptions and distributions, failure criteria and summarizes the simulation results and findings.

### **5.1 Crack Propagation Simulation Process**

In order to incorporate uncertainty into the crack propagation, the simulation proposed contains nested iterative loops that samples from the model parameter sets and then from the initial distributions. The entire simulation process is described in a flow chart in Figure 5.1.

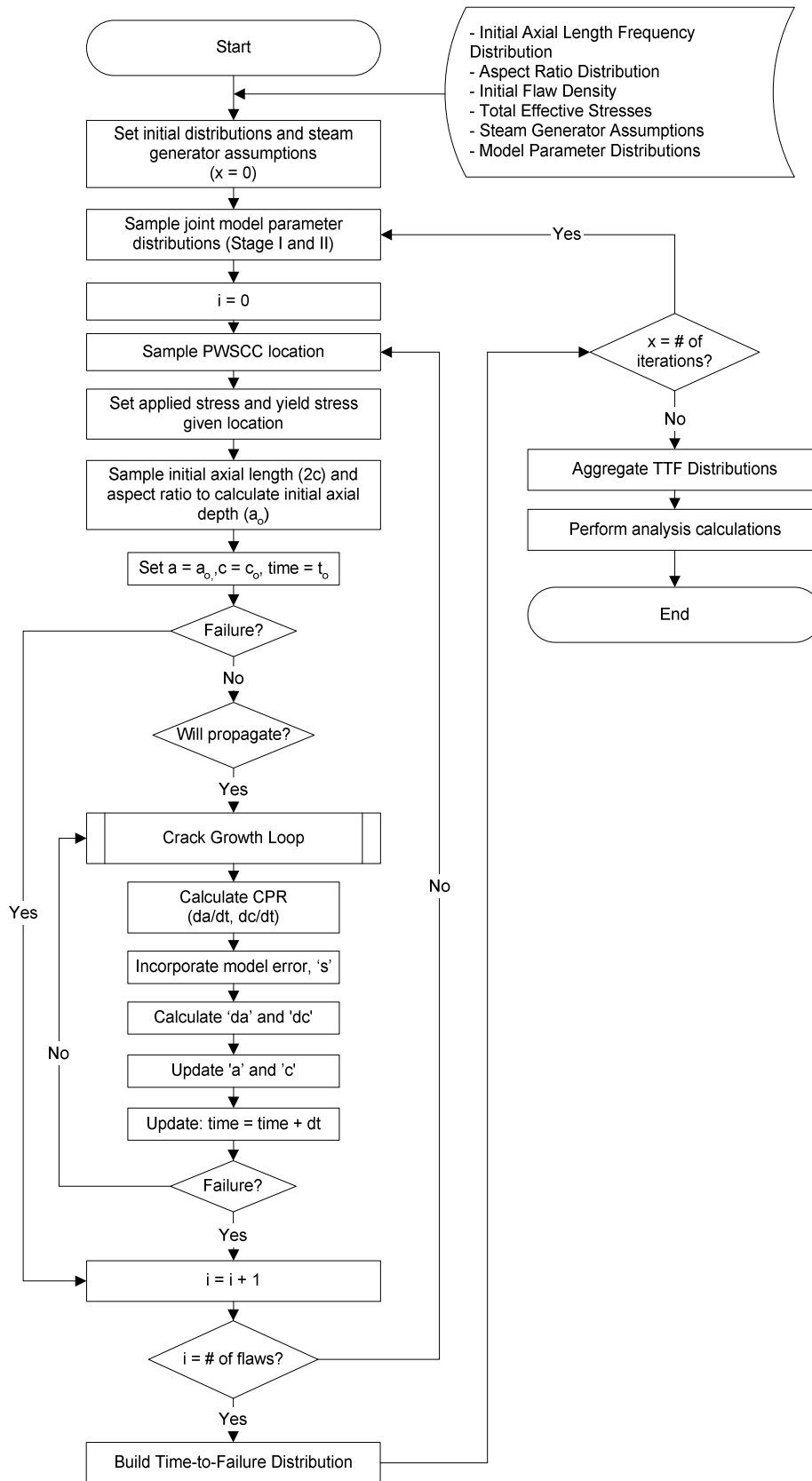


Figure 5.1 - Crack propagation simulation flow chart

The simulation starts by setting the steam generator assumptions and conditions as well as importing the initial distributions, which includes the joint model parameter distributions. In the first loop, the simulation samples the model parameters for both Stage I and Stage II. Using these parameters, the model is assumed to represent the calculated stress corrosion crack propagation rate. Keeping the model constant, the location of the cracking is randomly chosen between the expansion transition region, the tube support plate interactions and the U-bend regions. The simulation sets the appropriate applied stress and yield stresses depending on the crack location and samples the initial distribution to determine initial crack depth and length. Before starting the crack propagation, the simulation checks to make sure that the sampled initial crack size is within the crack propagation stage using the failure criterion (Section 5.3). If there is SCC propagation, the sub-loop iteratively grows the crack by using the crack propagation rate calculated by the model. When the crack finally fails, the simulation exits the crack growth nested loop. The process continues by sampling once again another initial crack size. After a number of iterations, the uncertainty of the initial distribution is captured given a crack propagation model with a constant set of model parameters. At this point, the main loop is performed again by sampling another set of model parameters. By repeating the entire loop, the simulation takes into consideration the uncertainty of the model parameters. As such, the simulation at this point yields a number of distributions. By aggregating them, the simulation can result in an average time-to-failure distribution. The simulation process is executed through a developed MATLAB code and can be found in Appendix C.

## 5.2 Initial Assumptions and Distributions

Several points must be emphasized regarding the proposed simulation process for stress corrosion cracking in Alloy 600 steam generator tubes. Firstly, the MATLAB simulation proposed in this research is developed specifically to model the crack propagation stage (See Section 2.2), since only the crack propagation mechanism is considered. This means that the following stages of stress corrosion cracking in Alloy 600 steam generator tubes are not modeled:

- Incubation Stage: *crack behavior from defect-free smooth surface to beginning of a crack*
- Crack Initiation Stage: *crack behavior from a small crack to a crack large enough to yield a stress intensity factor of  $9\text{MPa}\sqrt{\text{m}}$*
- Steam Generator Tube Rupture Behavior: *behavior of a 100% through-wall extent that ultimately causes a "steam generator tube rupture" as defined in Section 3.3*

In order to execute the simulation process, a number of assumptions and initial conditions must be introduced as shown in the crack propagation simulation flow chart. Some initial conditions are assumed to be constant values while others were provided as distributions.

The assumptions and initial conditions can be segmented in the following manner:

- Steam Generator Assumptions/Conditions
- Initial Crack Depth/Length Distributions
- Model Parameter Set Distributions

### 5.2.1 Steam Generator Assumptions/Conditions

Assumptions about the steam generator mechanical and environmental properties must be made in order to simulate SCC propagation. Table 5.1 below represents the operating conditions of a typical set of steam generators at a nuclear power plant.

**Table 5.1 - Steam Generator Mechanical/Environmental Properties**

<b>Steam Generator Mechanical/Environmental Properties</b>	
<i>Property</i>	<i>Value</i>
Number of SGs	2
Number of tubes	10025
Tube outside diameter [mm]	17.5
Tube inside diameter [mm]	15.5
Tube thickness [mm]	2
Tube length [m]	22
SG Tube material	Alloy 600
SG Tube treatment	LTMA
Number of tubesheet support plates	7
Primary side pressure [MPa]	17.24
Secondary side pressure [MPa]	5.67
Primary side temperature [Kelvin]	588
Primary water pH	7.3

It is assumed in this simulation that stress corrosion cracking in steam generator tubes in primary water environments occur axially in three regions: U-bends, Tubesheet Support Plate Intersections, and Expansion Transition. The expansion transition is assumed to be a full-depth hard-rolled expansion. As such, assumptions must be made about the flaw density, yield stress and total effective stress in the three areas. Table 5.2 summarizes these assumptions.

**Table 5.2 - PWSCC Region Assumptions**

<b>PWSCC Region Assumptions</b>	
<b>Expansion Transition Region</b>	
<i>Property</i>	<i>Value</i>
Number of flaws per affected tube <sup>2</sup>	16
Number of affected tubes per SG	10025
Total effective stress [MPa]	430
Yield Strength <sup>1</sup> [MPa]	390
Ultimate Strength <sup>4</sup> [MPa]	737
<b>Tubesheet Support Plate (TSP) Region</b>	
<i>Property</i>	<i>Value</i>
Number of flaws per affected tube <sup>2</sup>	34
Number of tubes affected per SG <sup>2</sup>	501
Total effective stress [MPa]	415
Yield Strength <sup>1</sup> [MPa]	478
Ultimate Strength <sup>4</sup> [MPa]	737
<b>U-Bend Region</b>	
<i>Property</i>	<i>Value</i>
Number of flaws per affected tube <sup>3</sup>	20
Number of tubes affected per SG	230
Total effective stress [MPa]	510
Yield Strength <sup>1</sup> [MPa]	513
Ultimate Strength <sup>4</sup> [MPa]	737

<sup>1</sup> Yield strength is calculated assuming the 2% CW at expansion transition, 7% CW at TSP with a dent, 9% at U-bend

<sup>2</sup> See reference [24]

<sup>3</sup> U-bend flaw density is estimated given flaw densities for expansion transition and TSP

<sup>4</sup> See reference [27]

For each iteration, the simulation chooses a random PWSCC location. Since the flaw density is not the same for each region, the probability of choosing each location is not equal. The MATLAB code (See Appendix C) builds the true distribution using the flaw densities. By sampling from this distribution, the probability of a crack occurring at each location is captured more accurately.

## 5.2.2 Initial Crack Length and Depth Distributions

The simulation proposed in this research is designed to represent the stress corrosion crack propagation stage only. Therefore, initial stress corrosion crack lengths and depths distributions are required to incorporate initiation time. Unfortunately, in-service stress corrosion crack initiation time is often difficult to obtain. As such, the simulation uses an available crack length distribution of the Ringhals Unit 4 steam generator. [45] This distribution is formulated from inspection data in 1994, which is 11 years after the nuclear power plant's commissioning year. Figure 5.2 shows the distribution of crack length used in simulation from a Ringhal 4 steam generator fitted with a gamma distribution with parameters  $\{\alpha = 3.393, \beta = 1.395\}$ .

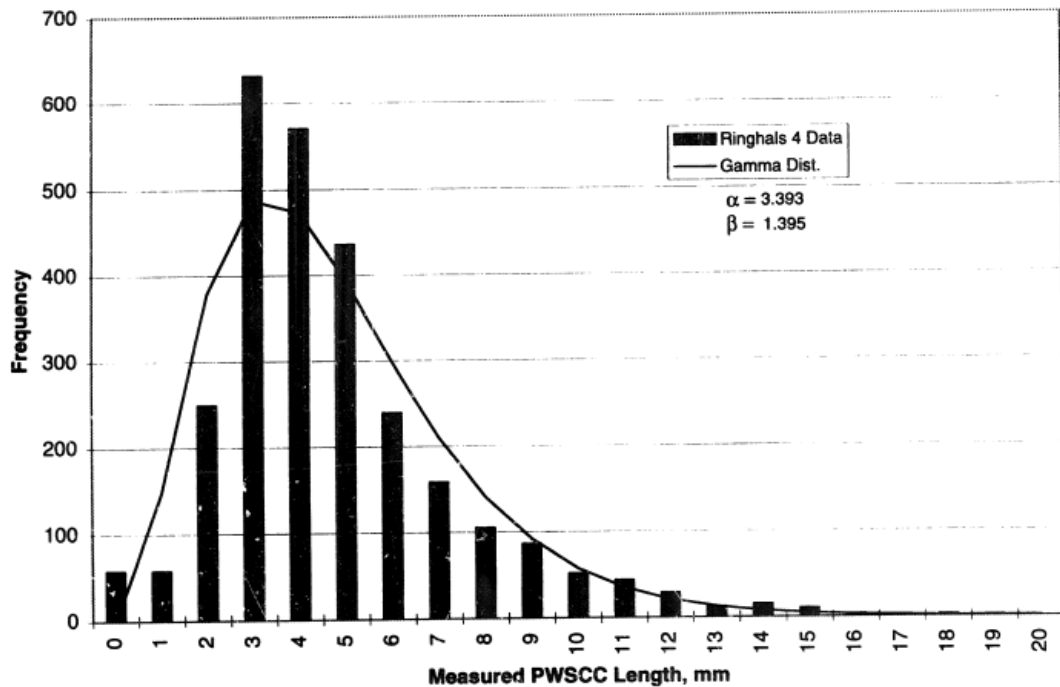


Figure 5.2 - Initial crack length distribution for simulation [45]

The simulation process also requires an initial crack depth distribution. Since no depth distribution was provided in conjunction with the crack length distribution, this research utilizes aspect ratios to convert the length distribution to a depth distribution.

Shin et al. [19] explored stress corrosion crack growth in Alloy 600 steam generator tubes at the expansion transition region through finite element analysis and determined that the aspect ratio of a crack penetrating the wall ranges from 0.24 to 0.35. Aspect ratio is defined by ' $a/c$ ' where ' $a$ ' is the crack depth and ' $c$ ' is half the length crack as shown in Figure 5.3. It is assumed that a semi-elliptical crack shape is retained as the crack propagates.

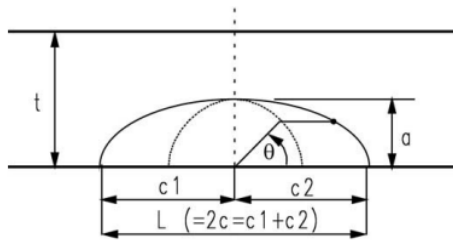


Figure 5.3 - Semi-elliptical crack penetrating through tube wall [19].

Assuming that the aspect ratio is uniformly distributed, the initial crack depth distribution is built by iteratively multiplying the crack length distribution by randomly generating aspect ratio values. Table 5.3 summarizes the initial assumptions used in the simulation process.

Table 5.3 – Initial assumptions used in simulation

<b>Initial Assumptions</b>		
<i>Property</i>	<i>Type</i>	<i>Parameters</i>
Initial Crack Length	Gamma Distribution	$\alpha = 3.393$ $\beta = 1.395$
Aspect Ratio	Uniform Continuous Distribution	$a = 0.24$ $b = 0.35$
Initial Time	Constant	11 years

### 5.2.3 Model Parameter Set Distributions

In order to apply the crack propagation rate uncertainty to the time-to-failure, the model parameter distributions are used directly in the simulation. Instead of classifying



the model parameter distributions for Stage I and II, the true distribution can be defined by the 50,000 and 80,000 data points for each model parameter set. By sampling from the 50,000 and 80,000 data points for Stage I and Stage II respectively, the shape and magnitude of the distributions are retained. See Section 4.4 for the model parameter estimation process.

### 5.3 Failure Criteria

As emphasized earlier in this chapter, the term "failure" is used in this research to describe a 100% through-wall crack. Evidently, the term is used to describe a number of tube states in literature depending on the author and the context of the research. Moreover, the simulation presented in this research considers crack propagation until the rupture of the remaining ligament across the thickness of the steam generator tube. As described in Section 3.3, a 100% through-wall extent is not necessarily considered a "steam generator tube rupture".

Due to pressure difference between the primary and secondary side, the tubes are prone to mechanical ligament failure at a certain length and depth. An analytical model incorporating the tube geometry, crack depth, crack length, operating conditions and flow stress is used to classify failure in the simulation.[46]

The failure model begins by determining the pressure required to fail a detect-free steam generator tube. The failure pressure can be calculated by:

$$P_b = \bar{\sigma} \log \left( 1 + \frac{h}{R} \right)$$

where  $h$  is the thickness of the tube,  $R$  is the inner tube radius and  $\bar{\sigma}$  is the flow stress.

The flow stress can be approximated by:

$$\bar{\sigma} = \frac{1}{2}(\sigma_{ys} + \sigma_{uts})$$

where  $\sigma_{ys}$  and  $\sigma_{uts}$  are the material yield strength and ultimate tensile strength, respectively.

For part-through wall axial cracks, the pressure required to fail the remaining ligament can be defined by:

$$P_{sc} = \frac{P_b}{m_p}$$

$$m_p = \frac{1 - \frac{a}{mh}}{1 - \frac{a}{h}}$$

$$m = 0.614 + 0.481\lambda + 0.386\exp(-1.25\lambda)$$

$$\lambda = \frac{1.82c}{\sqrt{R_m \cdot h}}$$

where  $a$  is the crack depth,  $c$  is half the crack length, and  $R_m$  is the mean tube radius.

When the effective pressure (pressure difference between primary and secondary sides) is greater than the  $P_{sc}$ , the crack is expected to mechanically propagate to a 100% through-wall crack very rapidly. The stability of 100% through-wall cracks is governed by another burst criteria that is not considered in this research.

This analytical model is implemented into the MATLAB code as a function to check for failure as the crack propagation is simulated. The function can be found in Appendix C.

## 5.4 Simulation Results and Findings

By using an initial distribution of the crack length at 11 years of steam generator operation, most of the flaws considered are within the crack propagation stage. As shown

in this section, the initial distribution includes a range of crack sizes. Some crack depths are too shallow to reside in the crack propagation stage given the total applied stresses while others cracks have already failed 100% through-wall. The remaining cracks reside in the crack propagation stage and can be modeled to failure.

After executing the MATLAB code, a number of pieces of information can be extracted from the results. To start, the distribution of PWSCC locations is calculated. Table 5.4 shows the probabilities for a crack initiating in each particular PWSCC region and also presents the total number of flaws per steam generator.

**Table 5.4 - PWSCC location probability**

<b>PWSCC Location</b>	<b>Probability</b>
Expansion Transition Region	0.565
Tubesheet Support Plate	0.419
U-Bend	0.016
<b>Total Cracks Per SG</b>	284,297

As shown, the location with the highest probability of crack initiation is at the expansion transition region followed closely by the tubesheet support plate intersection region. As expected, the probability of crack initiation at U-bends is very low relative to the other regions.

There were three types of cracks sampled from the initial distribution. The first type of crack is one that has is too small to reside in the crack propagation stage. The second type of crack is a crack that has already extended 100% through-wall but is still stable (the tube structure is still maintained). Finally, the third type of crack is one that resides in the crack propagation stage and can be propagated using the model.

If the total number of cracks sampled from the initial distribution for simulation is 80,000. At 11 years of reactor operation, 901 cracks have already propagated 100%

through the tube wall thickness, 77599 cracks are in the process of propagating through the tube wall thickness, and 1500 cracks still reside in the slow growing crack initiation stage.

By running the simulation for 100 samples of model parameters with 10 iterations each, it is able to provide a representation of the crack propagation behavior in the form of crack propagation rate as a function of stress intensity as shown in Figure 5.4.

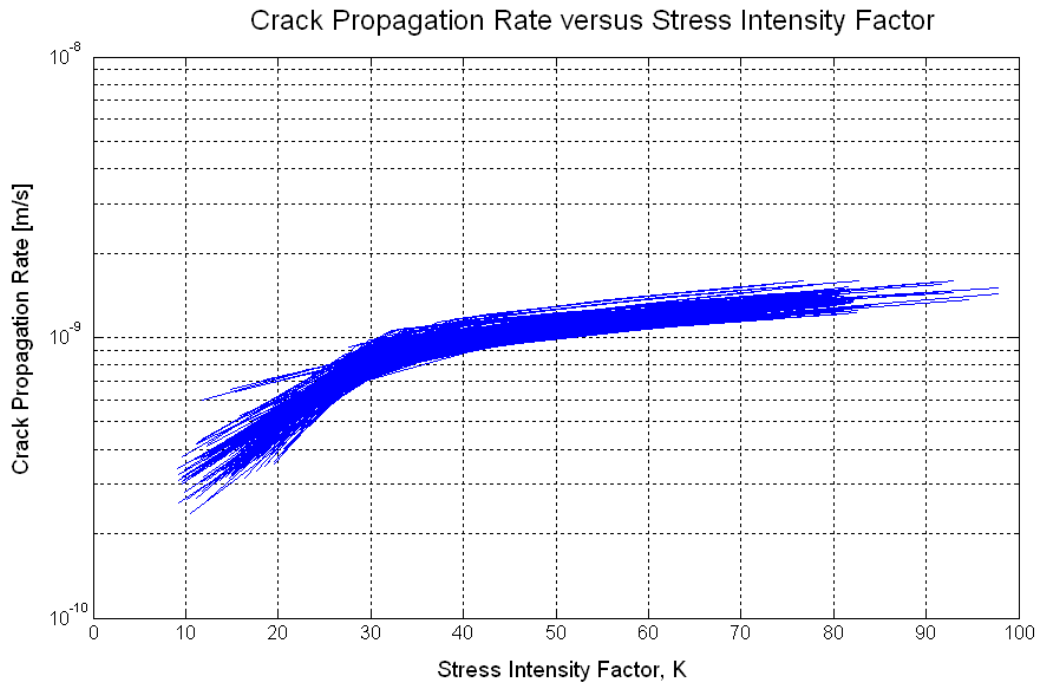


**Figure 5.4 - Crack Propagation Rate as a function of Stress Intensity Factor for simulation**

This curve incorporates the different locations of PWSCC which considers varying applied stresses and yield strengths. However, the simulation kept a constant environment of pH 7.3 and temperature 315°C. For comparison, the temperatures 315°C and 330°C for the same simulation are shown in Figure 5.5.

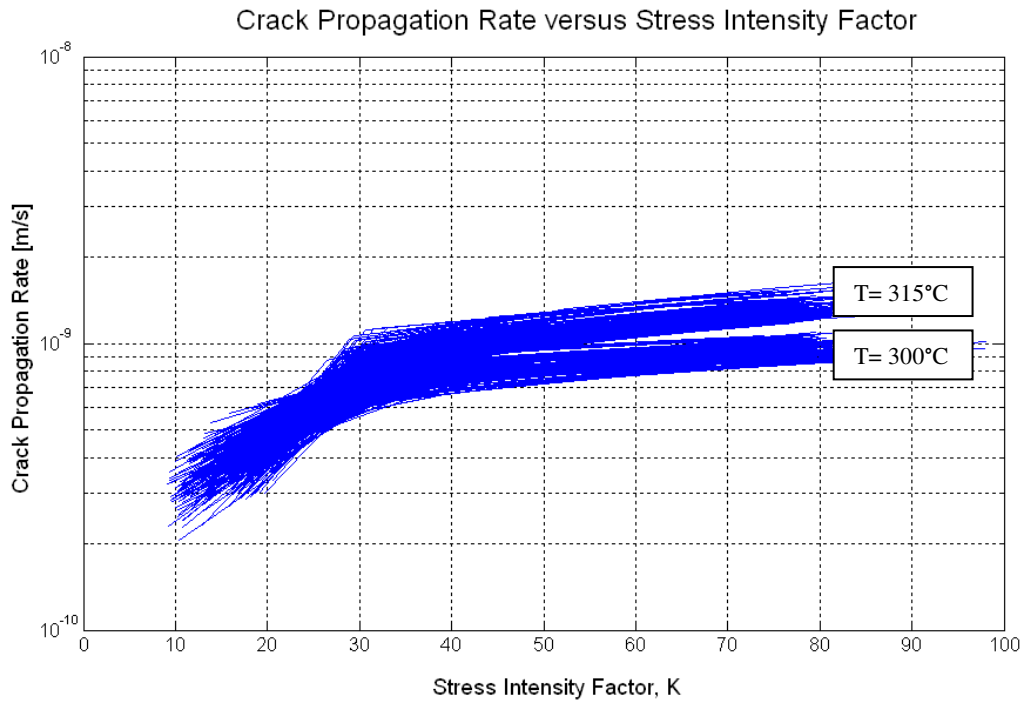


**Figure 5.5 – Crack propagation rate versus stress intensity factor for 300°C, 315°C**

The simulation process captured the SCC dependence on temperature. The figure demonstrates that the SCC propagation rates increase with the increase of operating temperature. The uncertainty distribution remains the same for each curve indicating that the simulation provides consistent results.

The progression of SCC propagation can be assessed by a crack depth versus time graph generated by 200 iterations of one sampled set of model parameters as shown in Figure 5.6. With 200 iterations shown in the diagram, it can already be seen that the mean time to 100% through-wall extent is a very short.

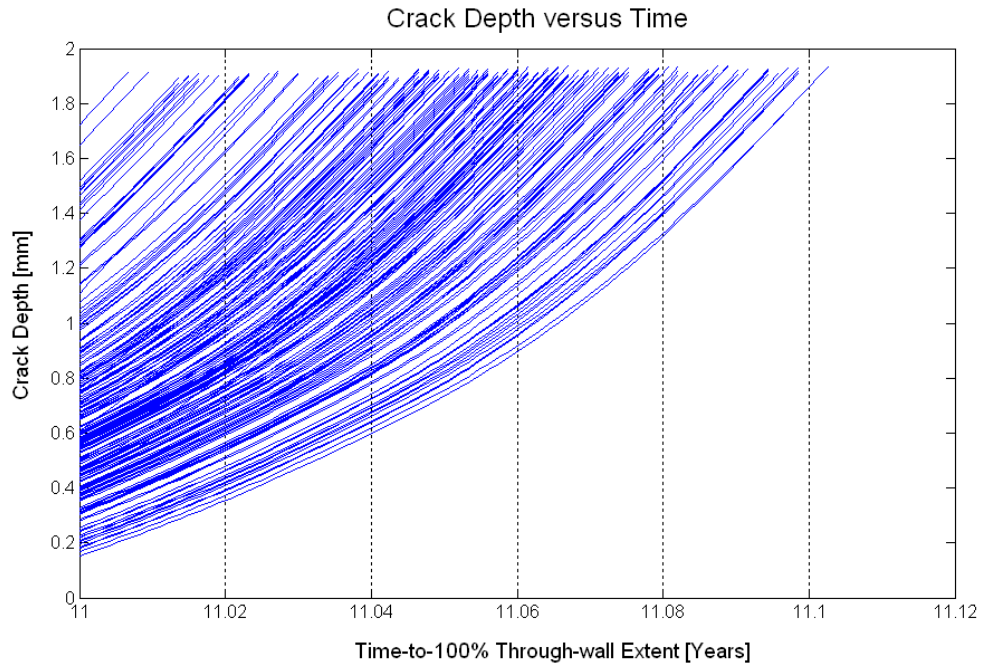


**Figure 5.6 - Crack depth as a function of time**

By collecting the failure times, which are schematically shown in Figure 5.6, the simulation builds the Time-to-100% TWE distribution in Figure 5.7, which is the distribution representing the time required for a single crack to propagate 100% through-wall.

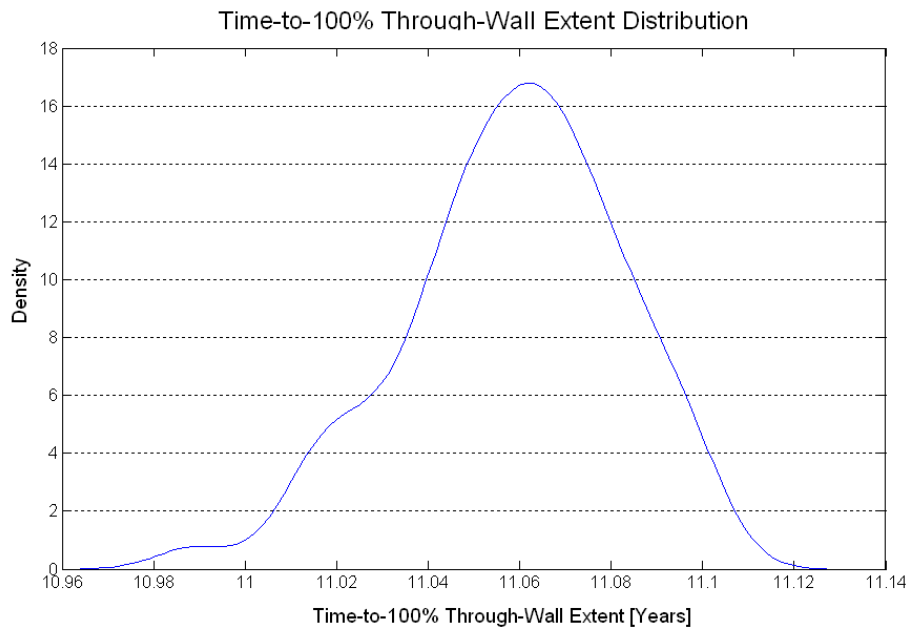


**Figure 5.7 - "Time-to-100% TWE" Distribution**

Ultimately, this distribution represents the uncertainty from the variation in initial crack sizes since the model parameters were only sampled once. In order to incorporate the uncertainty of the model parameters, multiple time-to-100% TWE distributions must be simulated. Figure 5.8 shows four overlapping distributions of different model parameter set samples.

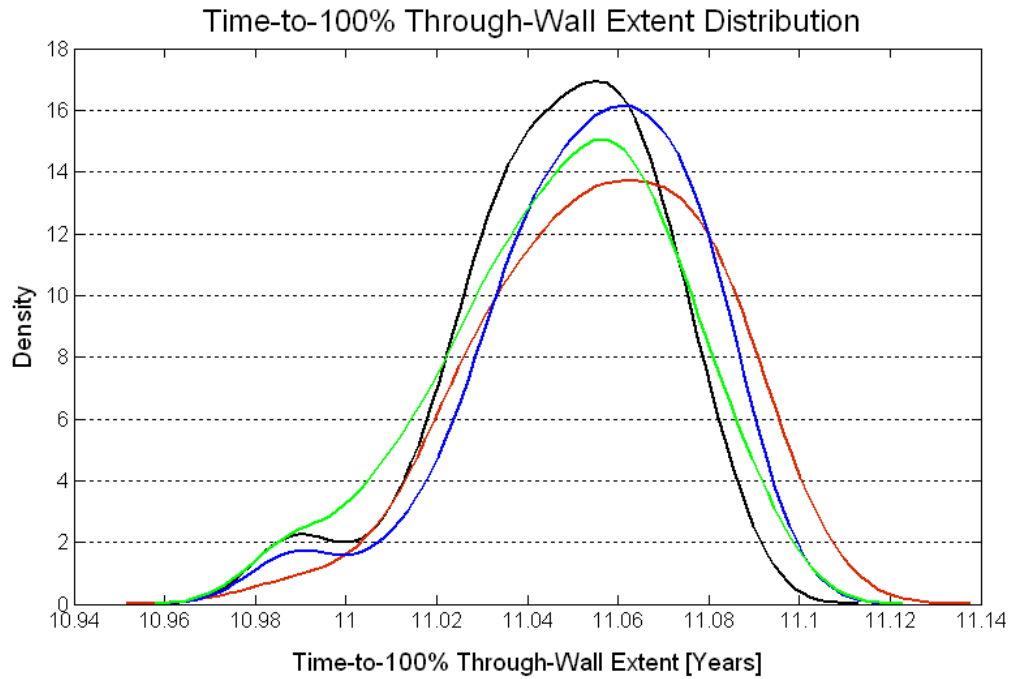


**Figure 5.8 - Overlapping Time-to-100% Through-Wall Extent Distributions**

While the figure above only shows four overlapping distributions, in order to incorporate the uncertainty of the model parameters, more model parameter sets would need to be sampled, thus leading to more overlapping distributions. After running the simulation 50 times, the overlapping distributions were aggregated by averaging. Figure 5.9 shows the averaged time-to-100% through-wall extent distribution.

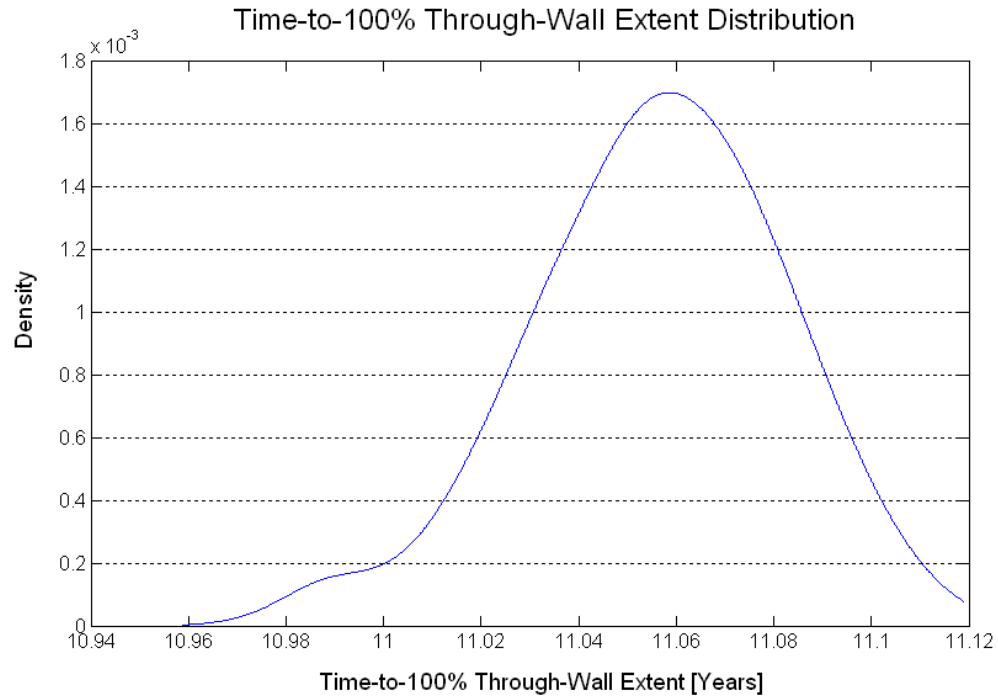


**Figure 5.9 - Aggregated Time-to-100% Through-Wall Extent Distribution**

The aggregated distribution above includes both the uncertainty from the variation of initial crack sizes and the uncertainty in model parameters. In this simulation, it is important to note that if the crack propagation rate was calculated to be less than zero due to the standard deviation measures, the crack growth is considered to be within the crack initiation stage and not modeled. Evidently, this means that the distributions developed here more accurately portray the crack propagation stage.

This simulation is also able to yield results for multiple cracks. As mentioned earlier, a steam generator tube rupture (SGTR) attributing to a loss-of-coolant (LOCA) may occur when a crack substantially contributes to a primary-to-secondary leak rate exceeding certain amounts. Some specifications have noted this amount to be 100 gallons per minute which refers to an SGTR-LOCA 1. In certain cases, 100 gallons per minute may be considered the normal makeup capacity of the plant, and exceeding that amount would also be considered a SGTR event. This value varies depending on the plant and



makeup pump specifications. Evidently, the definition of SGTR is shown to be ambiguous and non-standard. Thus, it is important to determine the most practical definition for use in modeling stress corrosion cracking.

However, this simulation only models crack propagation to failure, which is defined by a 100% through-wall extent. In order to expand this simulation to model SGTR occurrences, a number of factors must be considered. First of all, the crack behavior after 100% through-wall extent must be understood since there is now primary water flowing out of the crack. Next, a leak rate model must be assumed to estimate the amount of water leaking from the primary side into the secondary side based on the crack sizes. Finally, the simulation must incorporate regular inspection and maintenance schedules including plugging and sleeving when appropriate.

However, for the purpose of discussion, suppose more than one crack with a constant leak rate within a six hour time period is required to exceed the specified limit of 100 gallons per minute. This simulation process yields the appropriate data to determine the time required to achieve more than one crack in a set time period as shown in Figure 5.10.

Time Required for Leak Rate to Exceed Specified Limit for Multiple Cracks

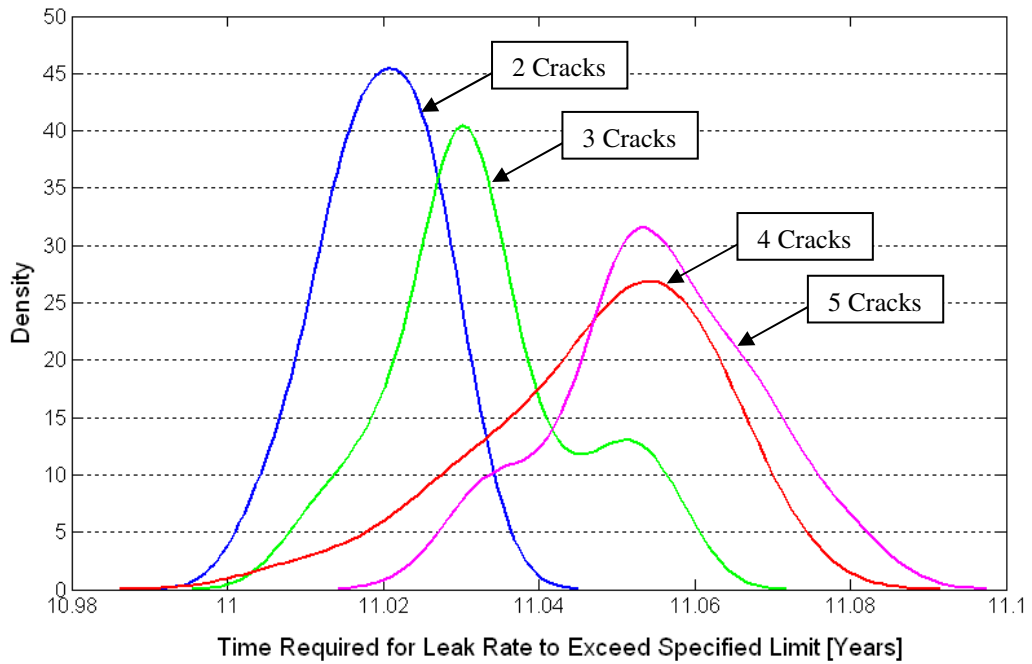


Figure 5.10 - Time Required for Leak Rate to Exceed Specified Limit for Multiple Cracks

As shown in the figure above, as the number of cracks required increases, the time required to exceed the leak rate limit also increases. This framework can be transferable to estimating SGTR and LOCA frequency.

## Chapter 6 Conclusion

The primary purpose of this research is to develop a probabilistic-mechanistic approach to modeling stress corrosion cracking propagation of Alloy 600 materials. This approach is applied to Alloy 600 LTMA steam generator tubes in primary water conditions at 315°C.

In order to understand the relevance of this approach, this research starts by exploring the complex fundamentals of stress corrosion cracking. This includes the factors that induce SCC, the stages of SCC, and SCC mechanisms and models. The three factors that combine to induce SCC are susceptible materials, their complementary corrosive environments, and surface tensile stresses. Susceptible materials are usually metal alloys such as stainless steels, aluminum alloys, and nickel-based alloys. Some of their corrosive environments include chlorides, alcohols and water, respectively. For most scenarios, the tensile stresses required for stress corrosion cracking are less than the macroscopic yield stress. In many cases however, the total applied stress includes residual stresses induced by manufacturing processes. Stress corrosion cracking can be understood in three separate consecutive stages starting with crack incubation which is the time period where the corrosion cracking conditions are established and stabilized. The next stage is the crack initiation stage, which is typically the longest stage of SCC, where a crack is formed from flaws. The final stage of SCC is the crack propagation stage. A crack enters this stage when it reaches a critical crack depth as defined by the threshold stress intensity factor ( $9\text{MPa}\sqrt{\text{m}}$  for Alloy 600 steam generator tubes). In this stage, the crack grows very quickly to failure. Since SCC is a degradation mechanism that can cause catastrophic and unwarned failures, many mechanisms and models have

been proposed to explain the cracking behavior. Some of them are very complex but can be applied to a range of SCC scenarios, while others have been empirically developed using experimental data for specific applications.

To provide a framework for the proposed probabilistic-mechanistic approach, an overview of nuclear power generation and steam generator tube degradation mechanisms were also included in this research. In summary, among multiple steam generator tube degradation mechanisms, stress corrosion cracking has been the main contributor for the last four decades. As such, it is important to understand how SCC affects steam generator tubes in order to preserve and improve the reliability of nuclear power plants as a whole.

The first part of the proposed approach is a developed empirical model for SCC propagation. This developed model is considered empirical as it requires experimental data to determine parameter values, but it includes mechanistic qualities because it considers the numerical relationships of the SCC-inducing factors. The proposed model adapts the MRP empirical model, which was originally developed for thick-wall Alloy 600 components in primary water, and expands it to include two other important factors: pH of the environment and the yield strength of the material. Using Bayesian regression techniques and an open source software called WinBUGS, the parameters for the model were estimated using available experimental data for SCC of Alloy 600 in primary water conditions. The regression analysis does not yield single values for the parameters but rather a joint distribution for the set of parameters. This allows for the proposed approach to capture the uncertainty and spread of the experimental data. The model parameter estimations for Stage I and Stage II can be found in Figure 4.6 and Figure 4.7. This

process is naturally generic since the same Bayesian estimation methods can be used with other SCC data to yield different parameter set results.

The second part of the proposed approach is a process by which crack propagation can be simulated. This research outlines the requirements for simulation such as the appropriate constants and initial conditions. A summary of the simulation process is as follows. The simulation starts by loading the proper initial distributions, model parameter distributions and constants for use in the virtual crack propagation. Afterwards, the first loop begins by sampling the joint model parameter distribution for both Stages I and II. Next, the location of the cracking is randomly chosen and the appropriate stresses are applied. The initial crack size is determined by sampling the initial crack length distribution and calculating the initial depth. After ensuring that the crack is within the crack propagation stage, the crack growth loop begins and grows the crack using the model. Once the crack fails based on the proposed failure criteria, the inner loop repeats by sampling a different cracking location and a different initial crack size. After a specified number of iterations, the inner loop closes and a time-to-100% through-wall extent distribution is built given the time to failures. The outer loop samples another set of model parameters from the joint distribution. The outer loop repeats for a set number of iterations and as a result constructs overlapping distributions. Ultimately, these distributions are aggregated by averaging and the final distribution is built.

It is important to mention that this simulation shed light on the importance of the initial distributions. The initial crack length distribution used in this application was built from inspection data of particular steam generator in the Ringhals 4 primary water reactor in 1994, 11 years after its commissioning. The manufacturing process for the Alloy 600

tubing was a low-temperature mill-annealing, now understood as more susceptible to SCC than high-temperature mill-annealing. The crack depth distribution was constructed using an aspect ratio assumption. Evidently, upper tails of the initial distributions included cracks that were already 100% through-wall. Therefore, it was impractical to use the results to determine the SCC frequency (number of 100% through-wall cracks per year). However, if the initial distribution did not contain any pre-failed cracks, the estimated SCC frequency can be determined by the inverse of the time to the first 100% through-wall extent.

In summary, the combination of the developed model and the simulation process provides a probabilistic approach to modeling stress corrosion cracking propagation of Alloy 600 materials. This approach brings forth an empirical model based on numerical relationship between cracking behavior and the SCC-inducing factors. Using the Bayesian regression analysis and the sampling methods in the simulation process, this approach allows for the incorporation of uncertainty in the form of distributions.

## Chapter 7 Future Work

It is recognized that this research only provides the framework to model the stress corrosion cracking behavior of Alloy 600 in the crack propagation stage. Evidently, in order to fully model stress corrosion cracking, all of the stages must be considered including crack incubation and crack initiation. Future steps in this area of research should include further mechanism and model exploration in these critical stages prior to crack propagation. Moreover, generic empirical models such as the one proposed in this research should be developed in order to describe the cracking behavior or crack growth rates during those stages. By incorporating the two stages into the simulation process, an initial distribution within the crack propagation stage would not be needed and the simulation would begin at a defect-free surface. This will provide a more comprehensive approach to physics-of-failure probabilistic modeling.

With regards to stress corrosion cracking of steam generator tubes specifically, future work should include an investigation of the exact degradation behavior from a 100% through-wall extent to a steam generator tube rupture (SGTR) as defined in Section 3.3. Not only will the degradation behavior govern the time between a 100% through-wall extent and a SGTR, other aspects such as inspection intervals, replacement, repair and plugging may also have significant contributions. As mentioned, the nuclear industry now uses historical data to estimate the SGTR frequency. Once the process between a crack and rupture is fully understood and quantified, the proposed probabilistic-mechanistic approach can be adapted and updated to estimate the SGTR frequency with uncertainty measures.

## Appendix A – Experimental Data

The table below lists the data used in the development of the proposed empirical model.

Source	Temp [K]	pH	CW [%]	$\sigma_{vs}$ [MPa]	K [MPa $\sqrt{m}$ ]	CPR [m/s]
[1]	603	5.2	1.57	389	12.2	6.53E-11
[1]	603	5.2	1.57	389	23	1.40E-10
[1]	603	5.2	1.575	389	53.4	9.10E-10
[1]	603	5.5	1.57	389	13.6	1.82E-11
[1]	603	5.5	1.57	389	22.2	4.00E-10
[1]	603	5.5	1.57	389	37.9	5.63E-10
[1]	603	5.5	1.575	389	37.9	5.63E-10
[1]	603	5.5	1.575	389	82.2	1.55E-09
[1]	603	5.6	1.57	389	10.2	1.54E-11
[1]	603	5.6	1.575	389	44	4.26E-10
[1]	603	5.6	1.575	389	89	1.38E-09
[1]	603	6.07	1.57	389	22.2	1.70E-11
[1]	603	6.07	1.575	389	42	5.26E-10
[1]	603	6.07	1.575	389	55.3	1.43E-10
[1]	603	6.07	1.575	389	64.2	5.15E-10
[1]	603	6.07	1.575	389	79.2	5.70E-10
[1]	603	6.07	1.575	389	90.7	1.09E-09
[1]	603	6.9	1.57	389	12.5	2.13E-11
[1]	603	6.9	1.575	389	44.2	5.30E-10
[1]	603	6.9	1.575	389	94.4	1.90E-09
[1]	603	7.3	1.57	389	13.5	3.00E-10
[1]	603	7.3	1.57	389	23	1.70E-10
[1]	603	7.3	1.57	389	38.7	7.40E-10
[1]	603	7.3	1.575	389	59.6	1.23E-09
[1]	603	7.3	1.575	389	78.9	1.78E-09
[1]	603	7.3	1.575	389	81	1.00E-09
[1]	603	7.4	1.57	389	10.5	1.22E-11
[1]	603	7.4	1.57	389	15.5	5.70E-11
[1]	603	7.4	1.57	389	25.8	3.63E-10
[1]	603	7.4	1.575	389	42	7.20E-10
[1]	603	7.4	1.575	389	84.5	1.18E-09
[1]	603	7.4	1.575	389	90	1.59E-09
[1]	603	7.4	1.575	389	90	1.28E-09
[1]	603	7.4	1.575	389	91	1.37E-09
[1]	603	7.6	1.57	389	11.9	1.27E-11
[1]	603	7.6	1.575	389	45	6.43E-10



[1]	603	7.95	1.57	389	13.6	1.90E-10
[1]	603	7.95	1.57	389	28.4	1.13E-09
[1]	603	7.95	1.575	389	57.1	3.56E-09
[1]	603	7.95	1.575	389	75.7	2.44E-09
[1]	603	7.95	1.575	389	81.4	2.16E-09
[1]	623	9	1.57	389	23.8	3.78E-10
[1]	623	9	1.57	389	37.8	1.96E-09
[1]	623	9	1.575	389	37.8	1.96E-09
[1]	623	9	1.575	389	51.4	3.13E-09
[1]	623	9	1.575	389	53.2	3.22E-09
[1]	623	9	1.575	389	62.7	3.54E-09
[1]	623	9	1.575	389	96.6	4.38E-09
[1]	623	9	1.575	389	101	6.28E-09
[2]	633	7.3	5	443	25.5	2.11E-09
[2]	633	7.3	5	443	25.5	2.11E-09
[2]	633	7.3	5	443	28	2.36E-09
[2]	633	7.3	5	443	28	2.36E-09
[2]	633	7.3	5	443	29.2	2.06E-09
[2]	633	7.3	5	443	29.2	2.06E-09
[2]	633	7.3	5	443	29.5	1.67E-09
[2]	633	7.3	5	443	29.5	1.67E-09
[3]	593	7.3	0	359	32.6	2.43E-10
[3]	593	7.3	0	359	32.6	2.43E-10
[3]	593	7.3	0	359	33.4	2.89E-10
[3]	593	7.3	0	359	33.4	2.89E-10
[3]	593	7.3	0	359	38.2	3.66E-10
[3]	593	7.3	0	359	38.2	3.66E-10
[3]	593	7.3	0	359	44.9	4.74E-10
[3]	593	7.3	0	359	59.2	7.42E-10

Sources: 1 - See Reference [40], 2 - See Reference [43], 3 – See Reference [44]

## Appendix B – WinBUGS Code

The following is the WinBUGS code used to estimate the model parameter sets for Stage

### I.

```
model{

  C ~ dunif(0,0.000000000005)
  n ~ dunif(0,10)
  s ~ dunif(0,0.0000001)
  m ~ dunif(0,10)
  Kth <- 9

  Z <- 10000
  R <- 8.134E-3 #This is a constant kJ/mol K
  Q <- 130
  Tref <- 588

  for (i in 1:N)
  {
    zeros[i] <- 0
    L[i] <- exp(-0.5*pow(((x[i,5] - C*exp(-(Q/R)*((1/x[i,1])-(1/Tref))))*pow((x[i,3]),m)*pow((x[i,4]-Kth),n))/s),2))/(s*pow(2*3.14159265,0.5))
    phi[i] <- -log(L[i]) + Z
    zeros[i] ~ dpois(phi[i])
  }
}
list(C = 0,0.000000000000000001, s = 0.000000001, m = 1, n = 2)
```

The following is the WinBUGS code used to estimate the model parameter sets for Stage

### II.

```
model{

  C ~ dunif(0,0.000000000005)
  n ~ dunif(0,10)
  s ~ dunif(0,0.0000001)
  b ~ dunif(0,10)
  m ~ dunif(0,10)
  Kth <- 9

  Z <- 10000
  R <- 8.134E-3
  Q <- 130
  Tref <- 588

  for (i in 1:N)
  {
```

```

zeros[i] <- 0

L[i] <- exp(-0.5*pow(((x[i,5] - C*exp(-(Q/R)*((1/x[i,1])-(
(1/Tref))))*pow((x[i,2]),b)*pow((x[i,3]),m)*pow((x[i,4]-
Kth),n))/s),2))/(s*pow(2*3.14159265,0.5))

phi[i] <- -log(L[i]) + Z

zeros[i] ~ dpois(phi[i])
}

list(C = 0,0.000000000000000001, s = 0.000000001, m = 1, n = 2, b =
0.5)

```

## Appendix C – MATLAB Code

The following is the MATLAB code used to represent the crack propagation simulation process.

```
% Crack Propagation MATLAB Code for SCC Alloy 600
% Developer: Gary Wu
% Version: 12
% Date: 04/19/2011
%
%-----
%           CODE STARTS HERE - New sampling
%-----

% clear and load model parameter distributions for Stage I and Stage II
clc
clear
load('s1_parameters.mat');
load('s2_parameters.mat');

% =====
% Define constants
% =====

% Steam Generator Assumptions/Constants
num_of_tubes = 10025; % number of tubes in SG
num_of_SGs = 2; % number of SGs
tube_OD = 0.0175; % [m] tube outside diameter
tube_ID = 0.0155; % [m] tube inside diameter
tube_thickness = 0.002; % [m]
tube_length = 22; % [m] tube length
p_pressure = 17.24; % [MPa] primary side pressure
s_pressure = 5.67; % [MPa] secondary side pressure
d_pressure = p_pressure - s_pressure; % [MPa] pressure differential
num_of_tsp = 7; % number of tubesheet support plates in SG
pH = 7.3; % pH of primary water environment
temp = 588; % [K] temperature of primary water 315C
sigma_uts = 737; % [MPa] ultimate tensile stress

% PWSCC Region Constants
% Expansion Transition Region - 2% cold working
exptrans_num_of_flaws = 16; % num of flaws in expansion transition
per affected tube
exptrans_sigma_ys = 390; % [MPa] yield strength at expansion region
exptrans_sigma_flow = 0.5*(exptrans_sigma_ys+sigma_uts); % exp
trans flow stress
exptrans_sigma_app = 430; % [MPa] applied+residual stress for
expansion trans region
exptrans_flaws = num_of_tubes*exptrans_num_of_flaws; % [MPa] total
exp. trans. flaws in a SG

% Tubesheet Support Plate Region - 7% CW
```

```

    tsp_num_of_flaws = 34; %num of flaws in tsp region per affected
    tube
    tsp_percent_tubes_affected = 0.05; %percent of tubes affected by
    denting
    tsp_sigma_ys = 478; %[MPa]yield strength at tsp region
    tsp_sigma_flow = 0.5*(tsp_sigma_ys+sigma_uts); % tsp flow stress
    tsp_sigma_app = 415; %[MPa] applied+residual stress for TSP region
    tsp_flaws =
    num_of_tubes*tsp_percent_tubes_affected*tsp_num_of_flaws*num_of_tsp;
    %total tsp flaws in a SG

    % U-Bend Region - 9% CW
    ubend_num_of_flaws = 20; %num of flaws in ubends per affected tube
    ubend_num_tubes_affected = 230; %U-Bend 1 and U-Bend 2 = 230 tubes;
    ubend_sigma_ys = 513; %[MPa]yield strength at U-Bend region
    ubend_sigma_flow = 0.5*(ubend_sigma_ys+sigma_uts); % ubend flow
    stress
    ubend_sigma_app = 510; %[MPa] applied+residual stress for U-Bend
    region
    ubend_flaws = ubend_num_tubes_affected*ubend_num_of_flaws; %total
    ubend flaws in a SG

    % Other Constants
    Kth = 9; %[MPaROOT(m)] threshold SCC intensity factor
    Y = 1; %Assume geometric constant is 1
    Tref = 588; %[Kelvin] Normalize to 315C
    Q = 130; %kJ/mol
    R = 0.008314; %[kJ/mol-K] Boltzman constant
    % =====

    % =====
    % Build flaw location and applied stress and distribution
    % =====

    ubend_flaw_norm = round(ubend_flaws/ubend_flaws);
    tsp_flaw_norm = round(tsp_flaws/ubend_flaws);
    exptrans_flaw_norm = round(exptrans_flaws/ubend_flaws);
    sum_flaws = ubend_flaw_norm+tsp_flaw_norm+exptrans_flaw_norm;
    order = transpose(randperm(sum_flaws)); %generate random ordering for
    flaws
    flawdist = zeros(sum_flaws,3); % col1: location[1-ubend, 2-tsp, 3-
    exptrans], col2: total eff. stress, col3: YS
    for count=1:ubend_flaw_norm
        flawdist(order(count),1)= 1; %U-bend
        flawdist(order(count),2)= ubend_sigma_app;
        flawdist(order(count),3)= ubend_sigma_ys;
    end
    for count=ubend_flaw_norm+1:ubend_flaw_norm+tsp_flaw_norm
        flawdist(order(count),1)= 2; %TSP
        flawdist(order(count),2)= tsp_sigma_app;
        flawdist(order(count),3)= tsp_sigma_ys;
    end
    for count=1+ubend_flaw_norm+tsp_flaw_norm:sum_flaws
        flawdist(order(count),1)= 3; %Expansion Transition
        flawdist(order(count),2)= exptrans_sigma_app;
        flawdist(order(count),3)= exptrans_sigma_ys;
    end
end

```

```

% =====

% =====
% Building Time-To-100%TW Iteration Loop
% =====

% Simulation conditions
iterations = 50; %number of samples for model parameter sets
iterations2 = 100; %number of samples for initial crack size

idtable = zeros(iterations,11); % model parameters used (8), prefail,
nprop
datatable = zeros(iterations2,iterations); % data matrix for 500
distributions
loca_matrix = zeros(iterations2,iterations); % matrix for locations

for cycle=1:iterations

    % retrieve random model parameters sets
    rands1 = random('unid',50000);
    rands2 = random('unid',80000);
    rands3 = random('unid',2);
    if(rands3 == 1)
        sign = 1;
    end
    if(rands3 == 2)
        sign = -1;
    end
    C = s1_parameters(rands1,2);
    n = s1_parameters(rands1,4);
    m = s1_parameters(rands1,3);
    s = sign*s1_parameters(rands1,6);
    Cs2 = s2_parameters(rands2,2);
    ns2 = s2_parameters(rands2,4);
    ms2 = s2_parameters(rands2,3);
    bs2 = s2_parameters(rands2,5);
    ss2 = sign*s2_parameters(rands2,6);

    %store
    idtable(cycle,1) = C;
    idtable(cycle,2) = n;
    idtable(cycle,3) = m;
    idtable(cycle,4) = s;
    idtable(cycle,5) = Cs2;
    idtable(cycle,6) = ns2;
    idtable(cycle,7) = ms2;
    idtable(cycle,8) = bs2;
    idtable(cycle,9) = ss2;

    % Initial distributions/constants
    length_initial_set = gamrnd(3.393,1.395,[iterations2,1])/1000;
    aspectratio_set = random('unif',0.24,0.35,[iterations2,1])/2;
    %aspect ratio = a/c

```

```

depth_initial_set = length_initial_set.*aspectratio_set;
%calculated depth
time_initial = 11; %[years] time at which the length/depth is
observed

prefail = 0; % number of flaws that already failed
noprop = 0; %number of flaws that do not propagate via SCC

for x = 1:iterations2

    % sample location
    location = random('unid',sum_flaws);

    % sample initial flaws
    aspectratio = aspectratio_set(x);
    a_initial = depth_initial_set(x);
    c_initial = length_initial_set(x);
    sigma_applied = flawdist(location,2);
    sigma_ys = flawdist(location,3);

    % check for initial failure
    fail = checkFail(a_initial,c_initial,sigma_ys);
    if(fail == 1) % if yes, add to pre-simulation failures
        prefail = prefail+1;
        ttf = -100;
    end

    if(fail == 0) % if not, propagate crack

        % Calculate initial K, dadt, and dc/dt
        K_initial = (sigma_applied*sqrt(pi()*(a_initial))*Y); %calc
K_initial [MPa*SQRT(m)]
        dt = 3600; %seconds to one loop 3600 = 1 hour, 86400 = 1
day, 2592000 = 1 month

        if(K_initial <= Kth) % if less than threshold, then the
crack will not propagate via PWSCC
            noprop = noprop + 1;
            ttf = -100;
        end

        % Only propagate if K_initial is greater than Kth
        if(K_initial > Kth)

            % Crack propagation
            time = 0;
            K = K_initial;
            a = a_initial;
            c = c_initial;
            dadt_s1 = (C*exp(-(Q/R)*((1/temp)-
(1/Tref)))*(sigma_ys^m)*((K-Kth)^n))+s; %calc new dadt [m/s]
            dadt_s2 = (Cs2*exp(-(Q/R)*((1/temp)-
(1/Tref)))*(pH^bs2)*(sigma_ys^ms2)*((K-Kth)^ns2))+ss2;
            if(dadt_s1 < 0)

```

```

        %dadt_s1 = (C*exp(-(Q/R)*((1/temp)-
(1/Tref)))*(sigma_ys^m)*((K-Kth)^n));
        dadt_s1 = 1E-11;
    end
    if(dadt_s2 < 0)
        %dadt_s2 = (Cs2*exp(-(Q/R)*((1/temp)-
(1/Tref)))*(pH^bs2)*(sigma_ys^ms2)*((K-Kth)^ns2));
        dadt_s2 = 1E-11;
    end
    if K < 20
        dadt = dadt_s1;
    end
    if (K >= 20) && (K < 30)
        trans = (K-20)/(30-20);
        dadt = dadt_s1*(1-trans) + dadt_s2*(trans);
    end
    if K >= 30
        dadt = dadt_s2;
    end

% -----
% Crack Propagation Loop
% -----
while(fail == 0)

    a_prior = a;
    time_prior = time;
    K_prior = K;
    dadt_prior = dadt;

    K = sigma_applied*sqrt(pi()*a)*Y; %calc new K value
    dadt_s1 = (C*exp(-(Q/R)*((1/temp)-
(1/Tref)))*(sigma_ys^m)*((K-Kth)^n))+s; %calc new dadt [m/s]
    dadt_s2 = (Cs2*exp(-(Q/R)*((1/temp)-
(1/Tref)))*(pH^bs2)*(sigma_ys^ms2)*((K-Kth)^ns2))+ss2;
    if(dadt_s1 < 0)
        %dadt_s1 = (C*exp(-(Q/R)*((1/temp)-
(1/Tref)))*(sigma_ys^m)*((K-Kth)^n));
        %dadt_s1 = 1E-12;
        break;
    end
    if(dadt_s2 < 0)
        %dadt_s2 = (Cs2*exp(-(Q/R)*((1/temp)-
(1/Tref)))*(pH^bs2)*(sigma_ys^ms2)*((K-Kth)^ns2));
        %dadt_s2 = 1E-12;
        break;
    end
    if K < 20
        dadt = dadt_s1;
    end
    if (K >= 20) && (K < 30)
        trans = (K-20)/(30-20);
        dadt = dadt_s1*(1-trans) + dadt_s2*(trans);
    end
    if K >= 30
        dadt = dadt_s2;
    end

```



```

end

% randomly select another aspect ratio for this
propagation
random_ac = random('unif',0.24,0.35);
dcdt = dadt/random_ac; %convert to dcdt using a/c
da = dadt*dt; %calc new da [m]
dc = dcdt*dt; %calc new dc [m]
a = a + da; %propagate crack length [m]
c = c + dc;
time = time + dt; %increase time

%hold on;
%plot(time/31536000,a);
%line([(time_prior/31536000)+11
(time/31536000)+11],[a_prior a]);

%line([K_prior K], [dadt_prior dadt]);
fail = checkFail(a,c,sigma_ys);
end
% -----
ttf = (time/3600);
end
end
ttft = ttf + time_initial*365*24;

%store
datatable(x,cycle) = ttft;
loca_matrix(x,cycle) = flawdist(location,1);
idtable(cycle,10) = prefail;
idtable(cycle,11) = noprop;

fprintf('Cycle: %d\n',cycle);
fprintf('Crack #: %d\n',x);
if(flawdist(location,1) == 1)
    fprintf('Location: U-Bend\n');
end
if(flawdist(location,1) == 2)
    fprintf('Location: TSP\n');
end
if(flawdist(location,1) == 3)
    fprintf('Location: Expansion Transition\n');
end
fprintf('a_initial 1: %f\n',a_initial*1000);
fprintf('c_initial 1: %f\n',c_initial*1000);
fprintf('ttf_scc [hours]: %f\n\n',ttft);
end
end

save('idtable.mat','idtable');
save('datatable.mat','datatable');
save('loca_matrix.mat','loca_matrix');

% =====

```

```

% checkFail() determines if the tube has failed 100%TW
% =====

function fail = checkFail(a,c,sigma_ys)

% Steam Generator Assumptions/Constants
R = 0.0155/2; %[m] tube inside radius
h = 0.002; %[m]
p_pressure = 17.24; %[MPa] primary side pressure
s_pressure = 5.67; %[MPa] secondary side pressure
d_pressure = p_pressure - s_pressure; %[MPa] pressure differential
sigma_uts = 737; %[MPa] ultimate tensile stress
sigma_bar = 0.5*(sigma_uts+sigma_ys);

if (a > h)
    fail = 1;
end
if (a <= h)
    Pb = sigma_bar*log(1+(h/R)); % failure pressure for unflawed tube

    % determine pressure required to fail remaining ligament. does not
    % mean that the tube will burst (fish-mouth) at this pressure
    Rm = R+(h/2);
    lamda = (1.82*c)/sqrt(Rm*h);
    m = 0.614 + 0.481*lamda + 0.386*exp(-1.25*lamda);
    mp = (1-(a/(m*h)))/(1-(a/h));
    Psc = Pb/mp;
    if (Psc < d_pressure)
        fail = 1;
    end
    if (Psc >= d_pressure)
        fail = 0;
    end
end

% -----

```

## Bibliography

- [1] Ralph I Stephens, Henry Otten Fuchs, Ali Fatemi, and Robert R Stephens, *Metal Fatigue in Engineering*, 2nd ed. United States of America: John Wiley & Sons Inc., 2001.
- [2] Joseph R Davis, Ed., *Corrosion - Understanding The Basics*. Materials Park, United States of America: ASM International, 2000.
- [3] R B Rebak and Z Szklarska-Smialowska, "The Mechanism of Stress Corrosion Cracking of Alloy 600 in High Temperature Water," *Corrosion Science*, vol. 38, no. 6, pp. 971-988, 1996.
- [4] T Shoji, S Suzuki, and R G Ballinger, "Theoretical Prediction of SCC Growth Behavior - Threshold and Plateau Growth Rate," in *International Symposium on Environmental Degradation of Materials in Nuclear Power Systems - Water Reactors*, Breckenridge, 1995, pp. 881-891.
- [5] Peter M Scott, "An analysis of primary water stress corrosion cracking in PWR steam generators," in *NEA/CSNI-UNIPED Specialist Meeting*, 1991, pp. 5.6: 1-16.
- [6] Samuel A Bradford, *Corrosion Control*, 2nd ed. Materials Park, United States of America: CASTI Publishing, Inc, 2001.
- [7] Denny A Jones, *Principles and Prevention of Corrosion*, 2nd ed. Upper Saddle River, United States of America: Prentice-Hall, Inc., 1996.
- [8] Muhammad Abduh. (2008, January) Integrity Engineering. [Online].  
<http://abduh137.wordpress.com/2008/01/20/corrosion-morphology/>
- [9] Russell H Jones and R E Ricker, "Mechanisms of Stress-Corrosion Cracking," in

- Stress-Corrosion Cracking: Materials Performance and Evaluation*, Russell H Jones, Ed. Materials Park, United States of America: ASM International, 1992, ch. 1, pp. 1-40.
- [10] Son Le Hong, Claude Amzallag, and Angel Gelpi, "Modelling of Stress Corrosion Crack Initiation on Alloy 600 in Primary Water of PWRs," in *International Symposium of Environmental Degradation of Materials in Nuclear Power Systems - Water Reactors*, Newport Beach, 1999, pp. 115-122.
- [11] B W Brisson, R G Ballinger, and A R McIlree, "Intergranular Stress Corrosion Cracking Initiation and Growth in Mill-Annealed Alloy 600 Tubing in High-Temperature Caustic," *Corrosion Science*, pp. 504-514, July 1998.
- [12] A R McIlree, R B Rebak, and S Smialoska, "Relationship of stress intensity to crack growth rate of Alloy 600 in primary water," in *International Symposium Fontevraud II, Vol. 1*, 1990, pp. 258-267.
- [13] A Turnbull, L N McCarney, and S Zhou, "A model to predict the evolution of pitting corrosion and the pit-to-crack transition incorporating statistically distributed input parameters," *Corrosion Science*, vol. 48, pp. 2084-2105, 2006.
- [14] Y Kondo, "Prediction of Fatigue Crack Initiation Life Based on Pit Growth," *Corrosion*, vol. 45, pp. 7-11, 1989.
- [15] Omar Fernandes Aly, Miguel Mattar Neto, Arnaldo H Paes de Andrade, and Monica Schvartzman, "Study for Extension and Improvement on Modeling of Primary Water Stress Corrosion Cracking at Control Rod Drive Mechanism Nozzles of Pressurized Water Reactors," in *64th ABM Annual Congress*, Belo Horizonte, 2009.

- [16] Jose R Galvele, "A Stress Corrosion Cracking Mechanism Based on Surface Mobility," *Corrosion Science*, vol. 27, no. 1, pp. 1-33, 1987.
- [17] Peter L Andresen and Peter F Ford, "Life prediction by mechanistic modeling and system monitoring of environmental cracking of iron and nickel alloys in aqueous systems," *Materials Science and Engineering: A*, vol. 103, no. 1, pp. 167-184, August 1988.
- [18] Koichi Saito and Jiro Kuniya, "Mechanochemical model to predict stress corrosion cracking growth of stainless steel in high temperature water," *Corrosion Science*, vol. 43, pp. 1751-1766, 2001.
- [19] Kyu In Shin, Jai Hak Park, Hong-Deok Kim, and Han-Sub Chung, "Simulation of stress corrosion crack growth in steam generator tubes," *Nuclear Engineering and Design*, vol. 214, pp. 91-101, 2002.
- [20] J Hicking, A McIlree, and R Pathania, "Crack Growth Rates for Evaluating Primary Water Stress Corrosion Cracking (PWSCC) of Thick-Wall Alloy 600 Material (MRP-55)," Electric Power Research Institute, Palo Alto, NRC ADAMS Accession No. ML023010510, 2002.
- [21] S Majumdar, "ANL/CANTIA: A Computer Code for Steam Generator Integrity Assessments," Nuclear Regulatory Commission, Washington DC, NUREG/CR NUREG/CR-6786, 2002.
- [22] U.S. Department of Energy, "The History of Nuclear Energy," U.S. Department of Energy, Educational Publication DOE/NE-0088,.
- [23] U.S. Energy Information Administration. (2011, February) U.S. Energy Information

Administration: Independent Statistics & Analysis. [Online].

<http://www.eia.doe.gov/totalenergy/>

- [24] Peter N Paine, "Steam Generator Reference Book, Revision 1," Electric Power Research Institute (ERPI), Palo Alto, Reference Book RP2858; RP4004, 1994.
- [25] U.S. Nuclear Regulatory Commission, "Reactor Concepts Manual: Pressurized Water Reactor (PWR) Systems," U.S. Nuclear Regulatory Commission Technical Training Center, Washington DC, Educational Teaching Material 0603, 2007.
- [26] Kenneth Chuck Wade, "Steam Generator Degradation and Its Impact on Continued Operation of Pressurized Water Reactors in the United States," *Energy Information Administration/ Electric Power Monthly*, pp. ix-xxi, August 1995.
- [27] Precision Castparts Corp. (2008) SpecialMetals.com - The Alloy Experts. [Online].  
<http://www.specialmetals.com/>
- [28] P Millett, "PWR Primary Water Chemistry Guidelines - Volume 1, Revision 4," Electric Power Research Institute, Palo Alto, Water Chemistry Guidelines TR-105714-V1R4, 1999.
- [29] D R Diercks, W J Shack, and J Muscara, "Overview of steam generator tube degradation and integrity issues," *Nuclear Engineering and Design*, vol. 194, no. 1, pp. 19-30, November 1999.
- [30] U.S. Nuclear Regulatory Commission, "Indian Point Nuclear Generating Unit No. 2, Technical Evaluation Report of Steam Generator Tube Failure, Category C-3 Steam Generator Inspection Results, and Steam Generator Operational Assessment," U.S. Nuclear Regulatory Commission, Washington DC, Technical Evaluation Docket

No. 50-247, 2000.

- [31] R Tregoning, L Abramson, and P Scott, "Estimating Loss-of-Coolant Accident (LOCA) Frequencies Through the Elicitation Process," U.S. Nuclear Regulatory Commission, Washington DC, NUREG/CR NUREG-1829, 2008.
- [32] Charles E Rossi, "NRC Information Notice No. 91-43: Recent incidents involving rapid increases in primary-to-secondary leak rate," U.S. Nuclear Regulatory Commission, Washington DC, NRC Information Notice 91-43, 1991.
- [33] Brian K Grimes, "NRC Information Notice 94-62: Operational Experience on Steam Generator Tube Leaks and Ruptures," U.S. Nuclear Regulatory Commission, Washington DC, Information Notice ML031060406, 1994.
- [34] V N Shah et al., "Assessment of primary water stress corrosion cracking of PWR steam generator tubes," *Nuclear Engineering and Design*, vol. 134, pp. 199-215, 1992.
- [35] G S Was and K Lian, "Role of Carbides in Stress Corrosion Cracking Resistance of Alloy 600 and Controlled-Purity Ni-16% Cr-9% Fe in Primary Water at 360C," *Corrosion*, vol. 54, no. 9, pp. 675-688, 1998.
- [36] J A Gorman, R A Ogren, and N J Paine, "Correlation of Temperature with Steam Generator Tube Corrosion Experience," in *International Symposium of Environmental Degradation of Materials in Nuclear Power Systems - Water Reactors*, La Grange park, 1991, pp. 609-612.
- [37] R B Rebak, Z Xia, and Z Szklarska-Smialowska, "Effect of Temperature and Cold Work on the Crack Growth Rate of Alloy 600 in Primary Water," *Corrosion*, vol.

51, no. 9, pp. 689-697, 1995.

- [38] R B Rebak, A R McIlree, and Z Szklarska-Smialowska, "Effects of pH and Stress Intensity on Crack Growth Rate in Alloy 600 in Lithated + Borated Water at High Temperatures," in *International Symposium on Environmental Degradation of Materials in Nuclear Power Systems - Water Reactors*, Monterey, 1991, pp. 511-524.
- [39] Markus O Speidel and Ruth Magdowski, "Stress Corrosion Crack Growth in Alloy 600 Exposed to PWR and BWR Environments," *Corrosion*, 2000.
- [40] R B Rebak and Z Szklarska-Smialowska, "Influence of Stress Intensity and Loading Mode on Intergranular Stress Corrosion Cracking of Alloy 600 in Primary Waters of Pressurized Water Reactors," *Corrosion Science*, vol. 50, no. 5, pp. 378-393, May 1994.
- [41] P M Scott and Pierre Combrade, "On the Mechanism of Stress Corrosion Crack Initiation and Growth in Alloy 600 Exposed to PWR Water," in *International Conference on Environmental Degradation of Materials in Nuclear Systems*, Stevenson, 2003, pp. 29-35.
- [42] M K Cowles, "Review of WinBUGS 1.4," *The American Statistician*, vol. 58, no. 4, pp. 330-336, 2004.
- [43] T B Cassagne and A Gelpi, "Crack Growth Rate Measurements on Alloy 600 Steam Generator Tubes in Steam and Primary Water," in *International Conference on Environmental Degradation of Materials in Nuclear Power Systems - Water Reactors*, Monterey, 1991, p. 518.



- [44] John Paul Foster, Warren H Bamford, and Raj S Pathania, "Alloy 600 Crack Growth Rate Stress Intensity Dependence," in *International Conference on Environmental Degradation of Materials in Nuclear Power Systems - Water Reactors*, Stevenson, 2003, pp. 156-165.
- [45] J A Gorman, A P.L. Turner, M A Kreider, and J E Harris, "Estimating Probable Flaw Distributions in PWR Steam Generator Tubes," Nuclear Regulatory Commission/Argonne National Laboratory, Washington DC, NUREG/CR NUREG/CR-6521, 1998.
- [46] S Majumdar et al., "Failure Behavior of Internally Pressurized Flawed and Unflawed Steam Generator Tubing at High Temperatures - Experiments and Comparison With Model Predictions," U.S. Nuclear Regulatory Commission/Argonne National Laboratory, Washington DC, NUREG/CR NUREG/CR-6575, 1998.
- [47] R B Rebak and Z Szklarska-Smialowska, "Prediction of Crack Growth Rate in Service From Accelerated Tests in Laboratory for Steam Generator Alloy 600 Tubing," in *International Symposium on Plant Aging and Life Predictions of Corrodible Structures*, Sapporo, 1995, pp. 257-264.
- [48] R Bandy and D van Rooyen, "Quantitative examination of stress corrosion cracking of Alloy 600 in high temperature water," *Nuclear Engineering and Design*, vol. 86, no. 1, pp. 49-56, April 1985.